Scientific Research Publishing

ISSN: 2162-5360 Volume 7, Number 7, July 2017

Open Journal of Soil Science

ISSN: 2162-5360

9 772162 536000 07

www.scirp.org/journal/ojss

Journal Editorial Board

ISSN: 2162-5360 (Print), 2162-5379 (Online)
http://www.scirp.org/journal/ojss

Editor-in-Chief

Editorial Board

Scientific Research Publishing

Open Journal of Soil Science, 2017, 7, 111-171
http://www.scirp.org/journal/ojss
ISSN Online: 2162-5379
ISSN Print: 2162-5360

Table of Contents

Volume 7 Number 7 July 2017

Open Journal of Soil Science (OJSS)
Journal Information

SUBSCRIPTIONS

The *Open Journal of Soil Science* (Online at Scientific Research Publishing, www.SciRP.org) is published monthly by Scientific Research Publishing, Inc., USA.

Subscription rates:
Print: $69 per issue.
To subscribe, please contact Journals Subscriptions Department, E-mail: sub@scirp.org

SERVICES

Advertisements
Advertisement Sales Department, E-mail: service@scirp.org

Reprints (minimum quantity 100 copies)
Reprints Co-Ordinator, Scientific Research Publishing, Inc., USA.
E-mail: sub@scirp.org

COPYRIGHT

PRODUCTION INFORMATION

For manuscripts that have been accepted for publication, please contact:
E-mail: ojss@scirp.org

Scientific Research Publishing

Open Journal of Soil Science, 2017, 7, 111-117
http://www.scirp.org/journal/ojss
ISSN Online: 2162-5379
ISSN Print: 2162-5360

Fractal Kinetics Parameters Regulating Carbon Decomposition Rate under Contrasting Soil Management Systems

Léon E. Parent

Department of Soils and Agrifood Engineering, Université Laval, Québec, Canada
Email: leon-etienne.parent@fsaa.ulaval.ca

How to cite this paper: Parent, L.E. (2017) Fractal Kinetics Parameters Regulating Carbon Decomposition Rate under Contrasting Soil Management Systems. *Open Journal of Soil Science*, **7**, 111-117.
https://doi.org/10.4236/ojss.2017.77009

Received: May 23, 2017
Accepted: July 4, 2017
Published: July 7, 2017

Abstract

Agricultural soils can sequester and release large amounts of carbon. Accessibility of soil carbon to microbial attacks depends on biological, chemical, and physical protection mechanisms such as organic matter composition and particle size, soil aggregation, and chemical protection through the silt-clay-organic matter complex. While soil and organic matter are fractal objects controlling exposure of reactive surfaces to the environment, soil aggregation and biomass production and quality are regulated by agricultural practices. Organic matter decomposition in soil is generally described by the classical first-order kinetics equations fitted to define distinct carbon pools. By comparison, fractal kinetics assigns a coefficient to adjust time-dependent decomposition rate of total soil carbon to protection mechanisms. Our objective was to relate fractal parameters of organic matter decomposition to soil management systems. Retrieving published data, the decomposition of organic matter was modeled in a silt loam soil maintained under pasture, annual cropping or bare fallow during 11 years. The classical first-order kinetics model returned quadratic relationships indicating that reactive carbon decreased with time. Fractal kinetics rectified the relationships successfully. Initial decomposition rate (k_1 at $t = 1$) was 7×10^{-4} for pasture, 1×10^{-4} for annual cropping, and 0.5×10^{-4} for bare-soil fallow. Fractal coefficients h were 0.71, 0.45, and 0.25 for pasture, annual cropping and fallow, respectively. Due to aggregation, physical protection against microbial attacks was highest under pasture management, leading to higher carbon sequestration despite higher biomass production and "priming" effects. Parameters k_1 and h proved to be useful indicators for soil quality classification integrating the opposite effects of labile carbon decomposition and carbon protection mechanisms that regulate the decomposition rate of organic matter with time as driven by soil management practices.

Keywords

Aggregation, Annual Cropping, Carbon Pools, Carbon Sequestration, Fallow, Fractal Coefficient, Pasture, Soil Quality

1. Introduction

The soil is a huge reservoir of organic carbon approximately three times as large as the vegetation of terrestrial ecosystems and twice that of the atmosphere [1]. Properly managed soils can mitigate climate change through carbon sequestration and enhanced soil quality. Organic matter decomposition in soils is generally modeled by first-order kinetics that assigns rate coefficients to carbon pools defined by the model as labile to recalcitrant to decomposition [2] [3] [4] [5] [6]. The classical first-order kinetics equation assumes that each reaction rate is constant and that the mixture is homogeneous and fully dispersed [7].

However, most reactions in nature are fractal because they occur on low-dimensional heterogeneous surfaces where substrate accessibility, hence reaction rate, decreases with time [7] [8] [9]. Soil and organic matter are fractal objects [10] [11] that interact with each other [12]. Organic matter is a mixture of objects of various sizes and biochemical compositions [6] [13]. In batch reactions, surface area of particles and substrate reactivity per unit surface are enhanced by shredding and grinding, and by agitating the mixture [7]. Fractal kinetics [7] provides a means to regulate organic matter decomposition rate because carbon accessibility to microbial attacks changes with time due to "priming effect" of labile carbon [14] [15] [16] and to biological, chemical and physical protection mechanisms in the soil *in situ* [12] [17]. Indeed, biochemical composition of organic particles, organic particle size, soil aggregation and the silt-clay-organic matter complex limit surface areas of labile and recalcitrant organic matter materials. Biomass production and quality and soil aggregation are regulated by agricultural practices.

A hierarchical soil aggregation model for physical protection of organic matter against microbial attacks in a fractal soil system has been conceptualized by [18], described numerically by fractal [10] and Euclidean [19] geometry, and illustrated by [20]. Plant residues and fungi decompose into fragments and various substances, providing a nucleus for the formation of micro-aggregates less than 250 μm in diameter within macro-aggregates [21]. The micro-aggregates are mechanically strong while macro-aggregates may be destroyed by agricultural practices. By assigning a power coefficient to time to regulate the carbon decomposition rate in soils [22] [23] [24] [25], fractal kinetics can quantify the effect of tillage and crop rotation practices on enhancing or decreasing protection mechanisms against organic matter decomposition.

The aim of this paper was to relate fractal parameters of organic matter decomposition to agricultural practices regulating carbon sequestration in soils.

2. Material and Methods

2.1. Fractal Kinetics

First-order kinetics describes reactant disappearance as follows:

$$-\partial A/[A] = k\partial t \quad (1)$$

where A is concentration of the reactant remaining at time t and k is the first-order rate constant. The analytical solution of Equation (1) is as follows:

$$\ln\left(\frac{A}{A_o}\right) = -kt \quad (2)$$

where A concentration at time t is expressed as the proportion of initial reactant concentration A_o.

The rate "constant" k for reactions in diffusion-limited heterogeneous systems such as fractal objects has been shown both phenomenologically and theoretically to decrease with time as follows [7]:

$$k(t) = k_1 t^{-h} \quad (3)$$

where h is a fractal coefficient ($0 \le h \le 1$, $t \ge 1$) and k_1 is rate coefficient at $t = 1$. If $h \to 0$, reaction rate is maximum and kinetics gets closer to classical first-order Equation (2). Otherwise, the reaction follows fractal kinetics.

In organic matter decomposition studies, the fractal power coefficient p reduces reaction rate over time as follows [11] [22] [23] [24] [25]:

$$\ln(A) = \ln(A_o) - k(t)t = \ln(A_o) - kt^p \quad (4)$$

where $p = 1 - h$. The value of h is a measure of protection mechanisms against organic matter decomposition, and k_1 is maximum reaction rate at $t = 1$.

2.2. Computational Example

A computational example was retrieved from literature [26]. Briefly, a silt loam soil maintained under pasture, annual cropping or bare fallow during 11 consecutive years was sieved to less than 4 mm, incubated in the laboratory for 98 days, and monitored for CO_2 production. The $(C_{total} - C_{CO_2})/C_{total}$ ratio, where C_{total} is total carbon concentration and C_{CO_2} is cumulative CO_2 released during the incubation period, was log-transformed, then related to t for classical fractal kinetics or to t^{1-h} for fractal first-order kinetics. The value of h was iterated between 0 and 1 using Microsoft Excel until maximum r^2 value.

3. Results and discussion

3.1. Classical First-Order Kinetics

The soil under pasture released the largest amount of CO_2. The classical first-order kinetics showed significantly quadratic trends ($R^2_{adjusted}$ = 0.997 - 0.999) across treatments (**Figure 1**). Therefore, the reaction rates decreased with time, indicating that reactive surfaces became less accessible [7]. Classical first-order kinetics addresses this problem by splitting the curve into carbon pools (Thuriès

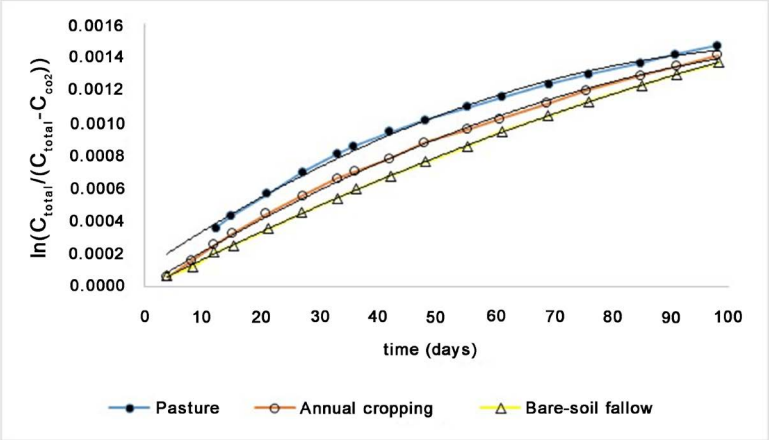

Figure 1. First-order kinetics of organic matter decomposition in soil under different soil management practices (bold colored lines) showing quadratic relationships (thin black lines). Data retrieved from [26].

et al., 2001). Because the clay-silt complex was similar across soils, microbial access to carbon pools was regulated by organic matter composition and encapsulation within aggregates. The soil under pasture that favored aggregation contained the largest amount of easily decomposable polysaccharides from recent plant residues while that under fallow showed smaller carbon content with higher concentration of recalcitrant polyphenols [26]. The sand fraction contained more easily biodegradable carbon forms compared to silt or clay.

3.2. Fractal kinetics

There were highly significant linear relationships between soil organic matter decomposition and t^{1-h} (Table 1). Initial decomposition rate k_1 was 14 times larger in the soil under pasture compared to bare-soil fallow, indicating large differences in labile carbon content due to higher biomass production under pasture. However, the higher was the h value, the smaller was $k_1 t^{1-h}$. Soil carbon decomposing at reduced rate needs not to be classified into carbon pools because fractal coefficient h not only accounts for chemical and physical protection but also for the recalcitrance of residual carbon that increases with time. A single total C pool decomposing at rate $k_1 t^{1-h}$ sufficed to describe organic matter decomposition in a fractal soil. Biochemical composition of organic matter materials provided an explanation for reduced reaction rate.

Despite "priming" effects by labile polysaccharides [14] [15] [16], carbon sequestration was highest under pasture management due to high biomass production by the sod and physical protection against microbial attacks through soil aggregation. In contrast, the h coefficient was lowest in the degraded bare-soil fallow where aggregation was low and biochemical carbon protection as polyphenols was high. The final result was carbon accumulation under pasture management compared to carbon depletion in the bare-soil fallow. As expected from the theory on carbon sequestration [18] [20] and in conformity with the fractal hypothesis [7], CO_2 release during organic matter decomposition is accelerated

Table 1. Fractal first-order parameters of organic matter decomposition in soil (data retrieved from [26].

Management practice	k_1	h	r^2
Pasture	7×10^{-4}	0.71	0.999
Annual crop	1×10^{-4}	0.45	0.999
Bare-soil fallow	0.5×10^{-4}	0.24	0.999

under conventional tillage that destroys soil aggregates and increases the exposure to microbial attacks of the formerly aggregate-protected organic matter [27]. As fractal coefficient decreased and soil particles were dispersed under fallow, the course of organic matter decomposition approached that of classical first-order kinetics. As fractal coefficient h increased due to soil aggregation, more carbon could be sequestered in the soil. The effect of conservation practices [28] and crop rotation [4] [29] on carbon sequestration can thus be compared using the h parameter.

Fractal parameters k_1 and h could also be used as soil quality indicators linked to soil functions like water regulation and partitioning, soil filtering and buffering, and nutrient storing and cycling [30]. High k_1 values reflected high respiration rate and microbial biomass, hence high biological activity. High h values reflected high organic carbon accumulation rate, content of particulate organic carbon, cation exchange capacity, and aggregation. As shown by k_1 and h, biological activity and aggregation, hence soil quality, were highest in the soil under pasture management and lowest in the soil under fallow.

4. Conclusion

The classical first-order kinetics that describes the decomposition of carbon pools at specific rate constants assumes that the medium is homogeneous and agitated. However, the soil is heterogeneous and structured, often showing fractal geometry. Fractal kinetics described successfully the course of total carbon decomposition in a fractal soil. Initial decomposition rate was highest in the pasture soil, which was well supplied with polysaccharides, and lowest in the fallow soil enriched in polyphenols. The pasture soil showed the highest h value due to higher aggregation that protects organic matter against microbial attacks. The h value regulated reaction rate as $k_1 t^{1-h}$, allowing organic matter to accumulate in the pasture soil despite higher initial decomposition rate compared with annual cropping and bare-soil fallow. Fractal parameters reflected soil quality and the effect of agricultural practices on soil carbon sequestration and release rates.

Acknowledgements

The author thanks the Natural Sciences and Engineering Research Council of Canada (NSERC-DG 2254) for financial support.

References

[1] Zhi, J., Jing, C., Lin, S., Zhang, C., Liu, Q., *et al.* (2014) Estimating Soil Organic

Carbon Stocks and Spatial Patterns with Statistical and GIS-based Methods. *PLoS ONE,* **9**, e97757. https://doi.org/10.1371/journal.pone.0097757

[2] Andrén, O. and Kätterer, T. (1997) ICBM: The Introductory Carbon Balance Model for Exploration of Soil Carbon Balances. *Ecological Modelling*, **7**, 1226-1236. https://doi.org/10.1890/1051-0761(1997)007[1226:iticbm]2.0.co;2

[3] Coleman, K. and Jenkinson, D.S. (2014) RothC—A Model for the Turnover of Carbon in Soils. Model Description and User Guide. Rothamsted Research, Harpenden, UK. https://www.rothamsted.ac.uk/sites/default/files/RothC_guide_WIN.pdf

[4] La Scala Jr., N., Lopes, A., Spokas, K., Archer, D.W. and Reicosky, D. (2009) First-Order Decay Models to Describe Soil C-CO_2 Loss after Rotary Tillage. *Scientia Agricola,* **66**, 650-657. https://doi.org/10.1590/S0103-90162009000500010

[5] Parton, W.J., Schimel, D.S., Cole, C.V. and Ojima, D.S. (1987) Analysis of Factors Controlling Soil Organic Matter Levels in Great Plains Grasslands. *Soil Science Society of America Journal,* **51**, 1173-1179. https://doi.org/10.2136/sssaj1987.03615995005100050015x

[6] Thuriès, L., Pansu, M., Feller, C., Herrmann, P. and Rémy, J.C. (2001) Kinetics of Added Organic Matter Decomposition in a Mediterranean Sandy Soil. *Soil Biology and Biochemistry*, **33**, 997-1010. https://doi.org/10.1016/S0038-0717(01)00003-7

[7] Kopelman, R. (1988) Fractal Reaction Kinetics. *Science,* **241**, 1620-1625. https://doi.org/10.1126/science.241.4873.1620

[8] Kopelman, R. (1986) Rate Process on Fractals: Theory, Simulations, Experiments. *Journal of Statistical Physics*, **42**, 185-200. https://doi.org/10.1007/BF01010846

[9] Savageau, M.A. (1995) Michaelis-Menten Mechanism Reconsidered: Implication of Fractal Kinetics. *Journal of theoretical Biology,* **176**, 115-124. https://doi.org/10.1006/jtbi.1995.0181

[10] Anderson, A.N., McBratney, A.B. and Crawford, J.W. (1998) Applications of Fractals to Soil Studies. *Advances in Agronomy,* **63**, 1-76.

[11] Dolgonosov, B.M. and Gubernatorova, T.N. (2007) Kinetics of the Enzymatic Decomposition of Macromolecules with a Fractal Structure. *Theoretical Foundations of Chemical Engineering*, **41**, 868-877. https://doi.org/10.1134/S0040579507060127

[12] Stewart, C.E., Plante, A.F., Paustian, K., Conant, R.T. and Six, J. (2008) Soil Carbon Saturation: Linking Concept and Measurable Carbon Pools. *Soil Science Society of America Journal*, **72**, 379-392. https://doi.org/10.2136/sssaj2007.0104

[13] Parent, S.-É. and Parent, L.E. (2015) Biochemical Fractionation of Soil Organic after Incorporation of Organic Residues. *Open Journal of Soil Science*, **5**, 135-143. https://doi.org/10.4236/ojss.2015.56013

[14] Chen, R., Senbayram, M., Blagodatsky, S., Myachina, O., Dittert, K., Lin, X., Blagodatskaya, E. and Kuzyakov, Y. (2014) Soil C and N Availability Determine the Priming Effect: Microbial N Mining and Stoichiometric Decomposition Theories. *Global Change Biology*, **20**, 2356-2367. https://doi.org/10.1111/gcb.12475

[15] Kuzyakov, Y. and Blagodatskaya (2015) Microbial Hotspots and Hot Moments in Soil: Concept & review. *Soil Biology and Biochemistry*, **83**, 184-199.

[16] Kuzyakov, Y., Friedel, J.K. and Stahr, K. (2000) Review of Mechanisms and Quantification of Priming Effects. *Soil Biology and Biochemistry*, **32**, 1485-1498.

[17] Plante, A.F. and McGill, W.B. (2002) Soil Aggregate Dynamics and the Retention of Organic Matter in Laboratory-Incubated Soil with Differing Simulated Tillage Frequencies. *Soil and Tillage Research*, **66**, 79-92.

[18] Oades, J.M. (1984) Soil Organic Matter and Structural Stability: Mechanisms and Implications for Management. *Plant and Soil*, **76**, 319-337. https://doi.org/10.1007/BF02205590

[19] Parent, L.E., de Almeida, C.X., Hernandes, A., Egozcue, J.J., Gülser, C., Bolinder, M.A., *et al.* (2012) Compositional Analysis for an Unbiased Measure of Soil Aggregation. *Geoderma*, **179-180**, 123-131.

[20] Six, J., Bossuyt, H., Degryze, S. and Denef, K. (2004) A History of Research on the Link between (Micro) Aggregates, Soil Biota, and Soil Organic Matter Dynamics. *Soil and Tillage Research*, **79**, 7-31.

[21] Six, J., Elliott, E.T. and Paustian, K. (2000) Soil Macroaggregate Turnover and Microaggregate Formation: a Mechanism for C Sequestration under No-Tillage Agriculture. *Soil Biology and Biochemistry*, **32**, 2099-2103.

[22] Bosatta, E. and Ågren, G.I. (1991) Dynamics of Carbon and Nitrogen in the Organic Matter of the Soil: a Generic Theory. *The American Naturalist*, **138**, 227-245. https://doi.org/10.1086/285213

[23] Kelly, J.M. and Beauchamp, J.J. (1987) Mass Loss and Nutrient Changes in Decomposing Upland oak and Mesic Mixed-Hardwood Leaf Litter. *Soil Science Society of America Journal*, **51**, 1616-1622. https://doi.org/10.2136/sssaj1987.03615995005100060038x

[24] Middleburg, J.J. (1989) A Simple Rate Model for Organic Matter Decomposition in Marine Sediments. *Geochimicaet Cosmochimica Acta*, **53**, 1577-1581.

[25] Wider, R.K. and Lang, G.E. (1982) A Critique of the Analytical Methods Used in Examining Decomposition Data Obtained from Litterbags. *Ecology*, **63**, 1636-1642. https://doi.org/10.2307/1940104

[26] Gregorich, E.G., Gillepsie, A.W., Beare, M.H., Curtin, D., Sanei, H. and Yanni, S.F. (2015) Evaluating Biodegradability of Soil Organic Matter by Its Thermal Stability and Chemical Composition. *Soil Biology and Biochemistry*, **91**, 182-191.

[27] Beare, M.H., Cabrera, M.L., Hendrix, P.F. and Coleman, D.C. (1994) Aggregate-Protected and Unprotected Organic Matter Pools in Conventional- and No-Tillage Soils. *Soil Science Society of America Journal*, **58**, 787-795. https://doi.org/10.2136/sssaj1994.03615995005800030021x

[28] Curtin, D., Wang, H., Selles, F., McConkey, B.G. and Campbell, C.A. (2000) Tillage Effects on Carbon Fluxes in Continuous Wheat and Fallow-Wheat Rotations. *Soil Science Society of America Journal*, **64**, 2080-2086. https://doi.org/10.2136/sssaj2000.6462080x

[29] Wright, A.L. and Hons, F.M. (2004) Soil Aggregation and Carbon and Nitrogen Storage under Soybean Cropping Sequences. *Soil Science Society of America Journal*, **68**, 507-513. https://doi.org/10.2136/sssaj2004.5070

[30] Karlen, D.L., Andrews, S.S. and Doran, J.W. (2001) Soil Quality: Current Concepts and Applications. *Advances in Agronomy*, **74**, 1-40.

Scientific Research Publishing

Open Journal of Soil Science, 2017, 7, 118-132
http://www.scirp.org/journal/ojss
ISSN Online: 2162-5379
ISSN Print: 2162-5360

Influence of Tillage Practices on Soil Physical Properties and Growth and Yield of Maize in Jabal al Akhdar, Libya

Gandura O. Abagandura[1]*, Gamal Eld-Deen Mohamed Nasr[2], Nouri Mosa Moumen[1]

[1]Soil and Water Department, Omar Al-Mukhtar University, Albida, Libya
[2]Department of Agricultural Engineering, Cairo University, Cairo, Egypt
Email: *gabagan@clemson.edu

How to cite this paper: Abagandura, G.O., Eld-Deen M. Nasr, G. and Moumen, N.M. (2017) Influence of Tillage Practices on Soil Physical Properties and Growth and Yield of Maize in Jabal al Akhdar, Libya. *Open Journal of Soil Science*, **7**, 118-132.
https://doi.org/10.4236/ojss.2017.77010

Received: May 19, 2017
Accepted: July 4, 2017
Published: July 7, 2017

Abstract

Different tillage practices are used for maize cropping in Libya. Yet, the effects of these practices on soil physical properties and maize growth and yield are not known. The objective of this study was to evaluate the effect of different tillage practices on soil physical properties and maize growth and yield in Libya. A field experiment was conducted in 2009 and repeated in 2010 using three tillage practices (conventional tillage (CT), ridge tillage (RT) and zero tillage (ZT)). Data about soil physical properties (penetration resistance (PR), bulk density (BD), total porosity (TP) and saturated hydraulic conductivity (Ks)) across soil depths, maize growth components (plant height, number of leaves, leaf area index and dry root weight) at 60, 75 and 125 days after planting, and maize yield (grain and stover) at harvest were collected and statistically analyzed in both years. To evaluate the effects of the tillage practices economically, the tillage operation cost and production cost were calculated. The results showed that at the surface layer (0 - 20 cm), CT had lower PR and lower BD, but higher TP and Ks compared to RT and ZT. At 20 - 40 cm and 40 - 60 cm depths, the lower PR and PD and higher TP and Ks were under ZT and RT compared to CT. All maize growth parameters at different times were highest for CT followed by RT and lowest for ZT. The CT practice presented the highest grain and stover yield followed by RT and ZT. However, harvest index was higher where ZT was applied. While tillage operation costs were the highest for CT followed by RT and ZT, the production costs were the highest for ZT followed by RT and CT. In general, the CT practice produced higher maize growth and yield, lower production cost, and higher tillage operation cost than those are planted using RT and ZT practices.

Keywords

Bulk Density, Conventional Tillage, Ridge Tillage, Tillage Cost, Zero Tillage

1. Introduction

Maize is considered one of the most important cereal crops in Libya [1], due to its greater demands for consumption and industrial purposes. Low soil organic matter and pests decrease maize production worldwide [2] [3] and Libya is not exception [4]. For this reason, Libya imported between 450,000 to 650,000 metric tons (18 to 26 million bushels) of maize in 2010 and estimated to import 450,000 tons (18 million bushels) in 2017 [5].

In addition, tillage management greatly affected maize growth in this country. Recent development in mechanization has differentially affected farmers in Africa including Libya. Many farmers use various tillage practices without being aware of the effect of these systems on soil physical properties and plant growth [6]. From the main author's experience in Libya, the farmers usually use moldered plow, chisel plow, and ridger before planting causing the formation of plow pans in some Libyan soils due to the pressure exerted by these machines [7]. Some Libyan farmers still plant without tillage to keep the organic matter from previous year on the surface to help hold the soil in place [6].

Soil tillage, as a necessary practice in crop production, can affect soil physical properties and affect plant growth as a result [8] [9] [10]. According to results of a 15 year experiment, zero tillage recorded higher bulk density and lower infiltration compared to conventional tillage [11]. Deep tillage had lower penetration resistance, lower soil bulk density but higher root length density on loam soil across depths compared to conventional tillage [12]. Conventional tillage achieved lower bulk density, higher water holding capacity and porosity that increased root depth and yield of maize compared to zero tillage [13].

However, there are other reports indicating that tillage practices did not affect soil physical properties and plant growth. No differences in bulk density, saturated hydraulic conductivity and maize yield were recorded between zero tillage and conventional tillage for silty clay loam soil [14]. According to [15], tillage practices had no effect on soil bulk density of the sandy soil surface (eight-year experiment).

Any tillage practice has to improve soil quality, which in turn improves the growth and yield of crops. Claims of different tillage practices can affect soil properties and plant growth are being promoted to Libyan farmers with minimal scientific support. To address this need, the objective of this study was to examine the influence of tillage practices on soil physical properties and maize growth and yield grown on clay loam soil in Libya.

2. Materials and Methods

2.1. Site Location

For this investigation, a two-year field study was conducted at the Omar Almukter Univrsity Center in Albida, Al Jabel Alkder, Libya (**Figure 1**) (32˚76'272"N, 21˚75'506"W, elevation 590 m) from July to November 2009 and repeated from June to September 2010. The topography was flat (<1% slope). The soil was a

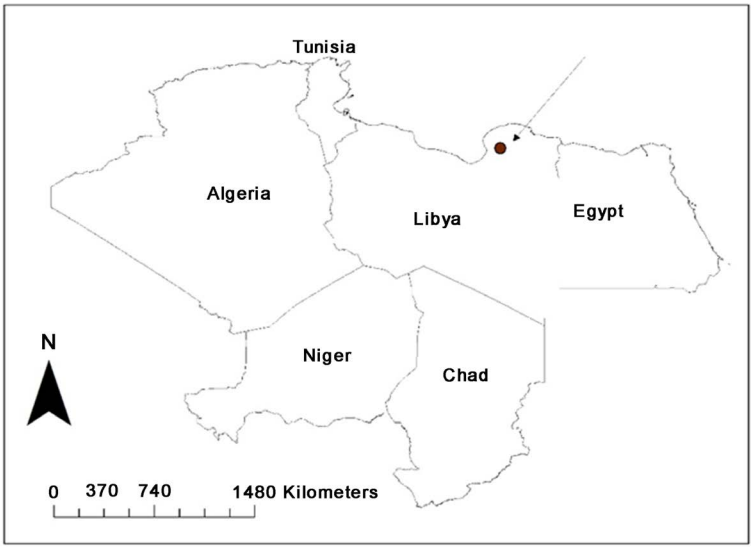

Figure 1. Geographical position of the study area.

mixed, superactive, calcareous, thermic Typic Xerorthents, Shedd Series (USDA classification), formed in residuum weathered from calcareous soft shale (moderately drained and has slow permeability). This area of the country has a plateau type climate with great rainfall and low temperature and used mostly for range and some grain with alternate fallow.

There was no crop growth and the field was left fallow two years prior to the start of the study. Prior to performing the tillage experiment, soil samples were collected from different locations at a depth of 0 - 20 cm. The soil texture was determined using hydrometer method [16]. Organic matter was determined by the modified Walkey-Black method as suggested by [17]. Available phosphorus (P) and potassium (K) were determined by the method of [18]. The soil in the experimental site was clay loam having an organic matter (6.25%), pH (7.30), available P (1.16 $mg \cdot kg^{-1}$), available K (0.05 $mg \cdot kg^{-1}$), and EC (0.38 $dS \cdot m^{-1}$) (average of five soil samples).

2.2. Tillage Implement Treatments

Four machines include of moldboard, chisel, land leveler and ridger were used in this investigation. A description of each machine is given in **Table 1**. A tractor with 55.1 kw and a mass of 2800 kg was used in both years. The manufacturing company of all machines is Simba Tractors Ltd, Nairobi, Kenya.

The experimental area was divided into three blocks 70 m long and 7 m wide (blocks separated by a 3 m spacing) used for each tillage practice. A small block (10 m long by 5 m wide) in the beginning of each tested block was used prior to the commencement of the actual test runs to enable the tractor and implement to reach the required speed. Three tillage practices were used to represent the standard primary tillage implements most commonly used for seedbed preparation in this region of the country. The tillage practices included conventional tillage (CT) performed using moldboard plow one pass followed by chisel plow one

Table 1. The machines description used in this study in 2009 and 2010.

Name	Width (m)	Weight (kg)	Specifications
Moldboard plow	1.05	400	Three furrows
Chisel plow	3.25	450	Thirteen curved shanks, seven in the front, and six in the back row
Lander leveler	1.02	200	Single plate
Ridger	1.8	300	NA

pass, lander leveler one pass and ridger one pass, ridge tillage (RT) performed using ridger one pass, and zero tillage (ZT). Treatments were replicated four times. The tillage speeds were as follow: 3.8 hr·km^{-1} for moldboard plow, 3.6 hr·km^{-1} for chisel plow one pass, 4.4 hr·km^{-1} for lander leveler, and 4.0 hr·km^{-1} for ridger.

2.3. Crop Cultivation

After the tillage practices, Zea mays L. cultivar (Arifiye) seeds were obtained from Agricultural Research Institute in Albida (Libya), planted by hand at a rate of 40 kg·ha^{-1} in three rows in each block (each block was divided into three rows) in both years. Surface drip irrigation (common in the region) was applied. Tensiometers (Spectrum Technologies, Inc., USA), one in each block, placed at 10 cm to 15 cm below the soil surface to indicate the soil water status. Before field installation, each tensiometer was calibrated. All blocks received the same management (planting, fertilizer, and weed control).

2.4. Soil Physical Properties Measurements

Soil physical properties (penetration resistance (PR) bulk density (BD), total porosity (TP) and saturated hydraulic conductivity (Ks) were measured two times, before tillage (**Table 2**) and after tillage when the maize was at grain physiological maturity, approximately four months from planting in both years [19]. The soil physical properties were determined from different locations in the field at 20 cm intervals starting from the surface down to a depth of 60 cm.

The PR were determined in the field at depths 0 - 20 cm and 20 - 40 cm and 40 - 60 cm using a hand-pushing penetrometer having maximum measurement range 5000 kPa and 80 cm depth. Soil penetrometer measurements were made by pushing the penetrometer vertically into the soil at each depth. Undisturbed core samples were collected at 0 - 20 cm, 20 - 40 cm, and 40 - 60 cm depths to measure the BD and Ks [14]. The BD and the Ks were determined on separated samples. BD was calculated using the procedure outlined by [20], then these values were used to calculate the TP using the following equation:

$$\text{Soil total porosity} = \left[\left(1-\text{BD}\right)/\text{soil particle density}\right] \quad (1)$$

the soil particle density assumed to be 2.65 g·cm^{-3}. The Ks was measured on soil cores in the laboratory using a constant head permeameter [15].

Table 2. Soil characteristics of the experiment before tillage as an average of the 2009 and 2010 experiments.

Depth (cm)	Penetration resistance ($kg \cdot cm^{-2}$)	Bulk density ($g \cdot cm^{-3}$)	Total porosity (%)	Saturated hydraulic conductivity ($cm \cdot h^{-1}$)
0 - 20	2.75	1.27	52.07	0.161
20 - 40	2.14	1.28	51.69	0.357
40 - 60	2.44	1.30	50.94	0.231

2.5. Growth and Yield Parameters Measurements

Percentage of emerged seedlings (PE) was calculated [21] for each tillage practice as follow:

$$\mathrm{PE} = \left[\left(\text{total emerged seedlings}/m\right)/\left(\text{number of seeds planted}/m\right)\right] \times 100 \quad (2)$$

five plants for each tillage practice were sampled randomly at 60, 75, and 120 days after planting to measure plant height, number of leaves, leaf area index and root weight. Plant height was measured as the vertical distance between the ground and the highest living part of the plant with a ruler. Number of leaves per plant was determined by counting all the leaves on each plant. The leaf area index was calculated [22] using the following equation:

$$\text{Leaf Area Index} = 0.75\left(\text{Leaf length} \times \text{Leaf width}\right) \quad (3)$$

for total dry shoot weight determination, the above ground samples were weighed and oven-dried at 80˚C and weighed again.

The dry root mass at various times and depths were determined. Maize roots were sampled with a soil core (a diameter of 10 cm and a height of 10 cm). The soil cores were taken to a depth of 60 cm in each block at four different locations. The cores were then taken to the lab and the soil and the roots were soaked in a solution containing 40 g/liter sodium hexametaphosphate in a 1:5 soil solution ratio [23]. Roots floated to the surface and were skimmed from the surface with a fine wire strainer. By subsequent washing in tap water roots and organic debris were separated. The roots were oven-dried at 80˚C and weighed.

At harvest (120 days after planting), grain and stover (above-ground biomass minus grain) yield were measured. Both the mass of grain and mass of stover were calculated after drying and converted to a per hectare basis at 14% moisture content [24]. Harvest index (%) was calculated on percentage basis by using the following formula:

$$\text{Harvest index} = \text{economic yield}/\text{biological yield} \quad (4)$$

climate data during the two growing seasons was collected from a weather station located approximately 500 m from the field.

2.6. Costs of Tillage Operation and Production Measurements

To estimate tillage operation cost, the cost associated with each tillage practice include machinery, fuel and labor was calculated totally as \$ ha^{-1} in both years.

Machinery costs were based on the data provided by Agricultural Research Institute in Albida, Libya. They were calculated according to the hours of use including costs for insurance, tax, and average repair costs. Fuel consumption was measured by using a secondary tank with a level marked tube and bulb with volume 140 cm^3 [25]. Labor was measured with a stopwatch for each tillage practice. No land costs included since land costs were the same across tillage practices [26]. Production cost ($\$\cdot ton^{-1}$ for grain + stover) include all variable costs for seed, lime, fertilizer, herbicides, and insecticides for each tillage practices were calculated.

2.7. Experimental Design and Data Analysis

A completely randomized block design was used in this study. Tillage was randomized within blocks. Data across the two years was assessed (residuals were homogeneous across years (Levene's test) and normal distributed (Shapiro-Wilk test), and then was statistically analyzed using the analysis of variance (ANOVA) to test the effects of tillage practices on the soil physical properties and maize growth and yield. All calculations were performed using SAS (SAS Institute Inc., North Carolina, USA). Year was first tested as a factor and found not significant for all metrics. Therefore, year was considered as a random factor in the model. Differences between the three tillage practices were compared by the Fisher LSD test. Differences between the means were considered to be statistically significant at $P < 0.05$.

3. Results and Discussion

3.1. Climate Conditions

Mean monthly temperature, precipitation and relative humidity during the study period in 2009 and 2010 are shown in **Figure 2**. The accumulated precipitation during the growing seasons was 7.4 cm in 2009 and 10.7 cm in 2011. The mean temperature during the growing season was 22.9˚C and 24˚C and the highest relative humidity was 72% and 71% in 2009 and 2010, respectively.

3.2. Soil Physical Properties

3.2.1. Penetration Resistance and Bulk Density

The PR and BD had similar trend to some extent at all depths which was expected because high BD produces high PR [27] [28]. At all depths, both parameters were significantly different among tillage practices (**Figure 3(a)**, **Figure 3(b)**).

As expected, the PR and the BD for the soil surface (0 - 20 cm) were the highest for ZT followed by RT, and the least was for CT (**Figure 3(a)**, **Figure 3(b)**), indicating that lack or minimum of disturbance produces an increase in both parameters measured at the soil surface. The lower PR and BD under CT compared to other tillage practices were probably due to tillage operations breaking the soil surface and producing loose soil [28] [29] [30]. Several studies documented that zero tillage recorded higher PR for the soil surface compared to tilled soil [31] [32] [33] [34] [35].

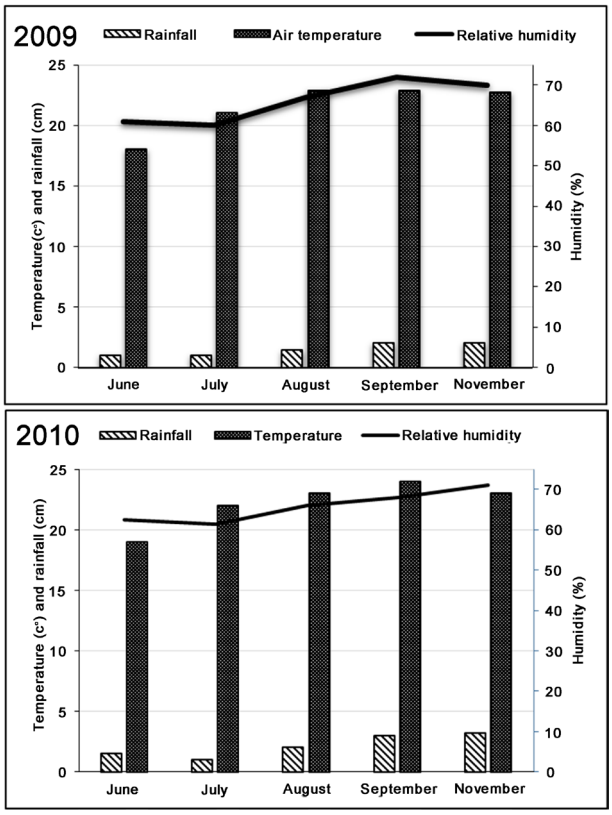

Figure 2. Mean monthly temperature, precipitation and humidity during the study period in 2009 and 2010.

For 20 - 40 cm and 40 - 60 cm depths, the lowest PR and PD were under ZT followed by RT and CT due to machinery weights used in CT (**Figure 3(a)**, **Figure 3(b)**). These results agree with [36] and [37] who reported that zero tillage led to higher PR and BD in the soil surface, but lower in both parameters in the deeper soil depths as compared to excessive tillage.

3.2.2. Total Porosity and Saturated Hydraulic Conductivity

The TP and Ks were found to have some similarity trend due to the fact that increasing soil TP enhances Ks and visa verse [38] [39]. Both parameters were influenced by the different tillage practices (**Figure 4(a)**, **Figure 4(b)**) at the three soil depths.

At 0 - 20 cm soil depth, while the highest TP and Ks were recorded under CT, the lowest were under ZT (**Figure 4(a)**, **Figure 4(b)**). [40] also found higher TP and Ks at the soil surface under conventional tillage compared to zero tillage. Similar to BD and RP, the trend of TP and Ks at the subsurface depths (20 - 40 cm, 40 - 60 cm) was reversed. The highest TP and Ks were recorded under ZT and the lowest were under CT (**Figure 4(a)**, **Figure 4(b)**). This result is probably due to machinery weights causing an increase in BD of the deeper depths under CT compared to ZT (**Figure 3(b)**) resulting decrease in TP and Ks under this practice. The relationship of BD and TP is reciprocal. As one increases, the other decreases.

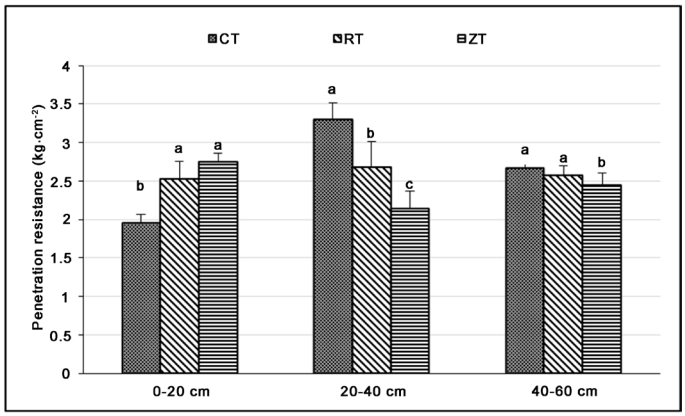

(a)

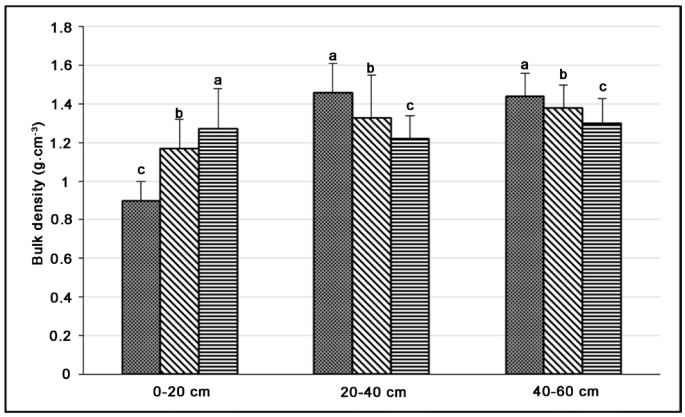

(b)

Figure 3. Penetration resistance (a) and bulk density (b) at different depths for the three tillage practices. Means are labelled with letters to denote statistical significance, a (largest), b (middle) and c (smallest). Within each column, means followed by the same letter are not significantly different at significant level = 0.05. The error bars represent the standard deviation. CT = moldboard plow, chisel plow, lander leveler and ridger, RT = ridger, ZT = no tillage.

3.3. Maize Growth and Yield

The PE differed among tillage practices ($p = 0.0206$). The highest PE was recoded under CT followed by RT and the lowest under ZT (**Figure 5**). The topsoil TP of the CT was higher compared to ZT (**Figure 4(a)**) which facilities free movement of air and moisture in the soil and thus increases the PE under CT. Similarly, [41] [42] found that zero tillage reduce the PE of maize compared to conventional tillage.

The tillage practices showed also significant difference in the maize growth. Plant height, number of leaves, leaf area index and dry weight of shoot at 60, 75, and 120 days after planting were the highest for CT and the lowest for ZT (**Table 3**).

The positive effect of tillage compared to zero tillage was observed in other maize growth studies. Taller plant [43] [44], higher number of leaves per plant and higher leaf area index [22] [45] of maize were found in tilled soil compared to zero tillage.

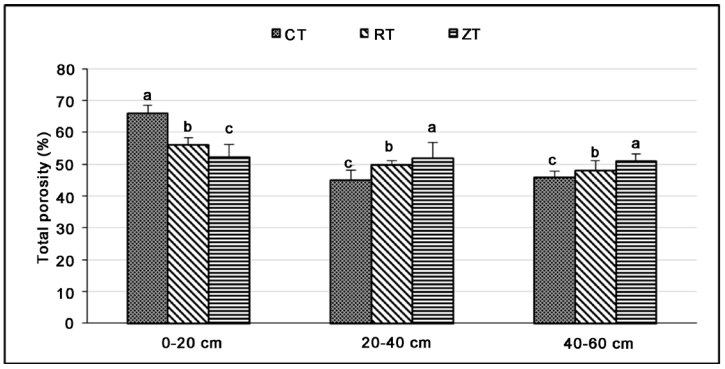

(a)

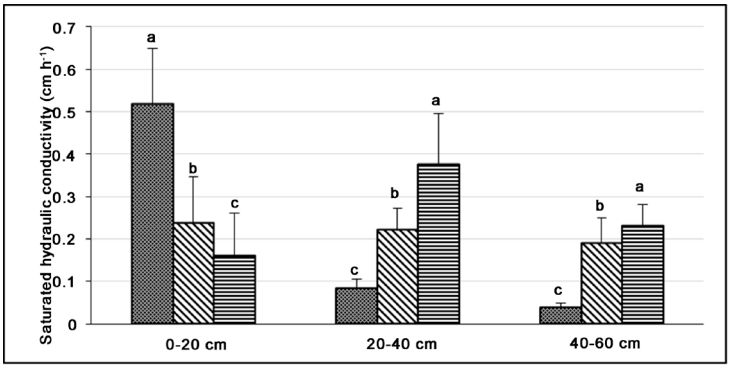

(b)

Figure 4. Total porosity (a) and saturated hydraulic conductivity (b) at different depths for the three tillage practices. Means are labelled with letters to denote statistical significance, a (largest), b (middle) and c (smallest). Within each column, means followed by the same letter are not significantly different at significant level = 0.05. The error bars represent the standard deviation. CT = moldboard plow, chisel plow, lander leveler and ridger, RT = ridger, ZT = no tillage.

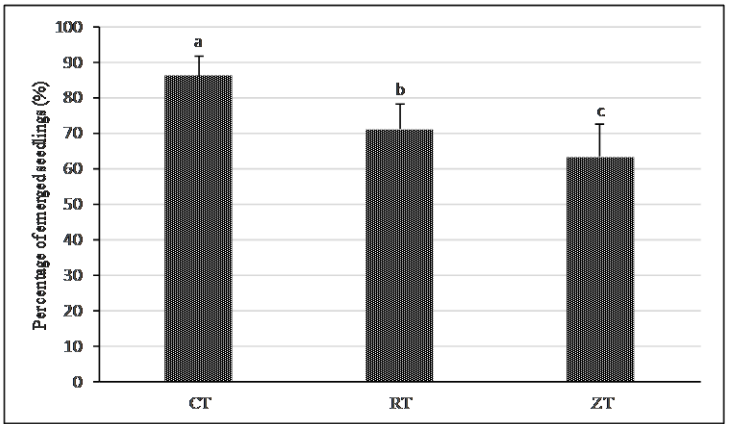

Figure 5. Percentage of emerged seedlings of maize for the three tillage practices. Means are labelled with letters to denote statistical significance, a (largest), b (middle) and c (smallest).Within each column, means followed by the same letter are not significantly different at significant level= 0.05. The error bars represent the standard deviation. CT = moldboard plow, chisel plow, lander leveler and ridger, RT = ridger, ZT = no tillage.

Table 3. Effect of tillage practices on maize growth at different times during the season.

Tillage	Days after planting		
	60	75	120
		Plant height (cm)	
CT	250.00 a	245.33 a	250.00 a
RT	160.00 b	200.33 b	204.91 b
ZT	150.33 c	192.00 c	200.33 c
P-value	0.0107	0.00839	0.0054
		Number of leaves	
CT	14.50 a	CT	14.50 a
RT	13.00 b	RT	13.00 b
ZT	12.33 c	ZT	12.33 c
P-value	0.0079	P-value	0.0079
		Leaf area index (cm^{-2})	
CT	1230.66 a	CT	1230.66 a
RT	1002.00 b	RT	1002.00 b
ZT	751.06 c	ZT	751.06 c
P-value	0.0116	P-value	0.0116
		Dry weight of shoot (g)	
CT	272.63 a	CT	272.63 a
RT	180.32 b	RT	180.32 b
ZT	157.53 c	ZT	157.53 c
P-value	0.0400	P-value	0.0400

Although the highest root dry mass across all depths at all times was found under CT and the lowest under ZT, these differences were not significant (data not shown). These results are similar to that of [46] who reported higher dry matter of root in conventional tillage compared to zero tillage in sandy loam soil.

The effect of tillage practices on grain and stover at harvest are shown in **Figure 6**. The ZT presented the lowest grain and stover yield in comparison with the other tillage practices (**Figure 6**). These results may be due to the lack of soil loosening for providing conditions favorable to crop growth and yield under ZT practice. [47] [22] also reported higher maize yield under CT compared to ZT practice. Soil tillage has a great influence upon the harvest index of maize recording lower harvest index (32%) when CT was applied compared to ZT (62%) and RT (53%). In other words, the physiological effectiveness of maize crop to partition the dry matter into its cost effective (grain) yield than generation of whole-plant biomass increased under ZT and RT compared to CT. These results are not in line with the findings of [48] who stated that higher harvest index was observed where conventional tillage was applied compared to minimum tillage. In other study [49], disking determined higher values of the harvest index than plowing.

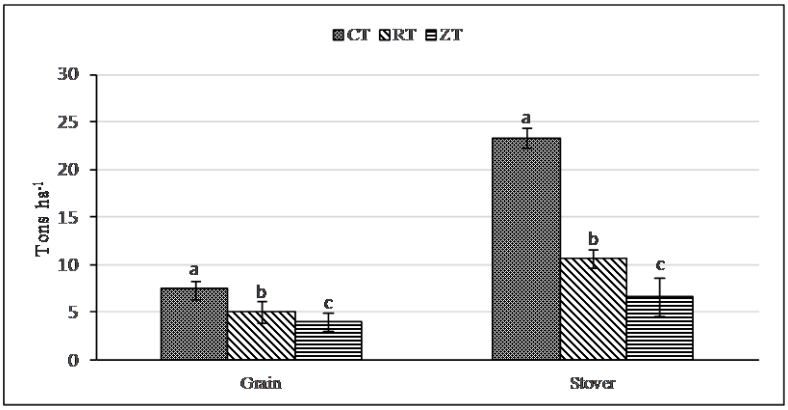

Figure 6. Maize grain and stover yield (ton·ha^{-1}) at harvest for the three tillage practices. Means are labelled with letters to denote statistical significance, a (largest), b (middle) and c (smallest). Within each column, means followed by the same letter are not significantly different at significant level = 0.05. The error bars represent the standard deviation. CT = moldboard plow, chisel plow, lander leveler and ridger, RT = ridger, ZT = no tillage.

3.4. Tillage Operation and Production Costs

Operation and production costs for each tillage practice are shown in Table 4. Estimates of total machinery, fuel and labor cost were the least for ZT practice compared to RT and CT (Table 4).

The operation tillage costs for CT were approximately $ 76.50 greater than for the RT (Table 4). On the other hand, the production costs were the highest for ZT compared to other practices. Although seed, fertilizer, lime and insecticide expenses were slightly similar among tillage practices, herbicide costs were higher in ZT and RT compared to CT (data not shown), probably due to the fact that zero or minimum tillage production rely exclusively on herbicides for weed control [50] [51].

4. Conclusions

Inappropriate tillage practices are considered a major constraint to maize production in Jabal al Akhdar, Libya. Based on the observed results:

- The three tillage practices had significant effects on the measured soil physical properties.
- Growth and development of maize were highly correlated with the type and degree of plowing.
- Harvest index was significantly affected by tillage practices and maximum harvest index was recorded where ZT was applied.
- The cost for seed preparation increased with increasing the usage of machines.
- The cost of the maize yield increased when soil left without tillage.

Long term tillage experiment (> two seasons) would be required to detect changes in soil physical properties and maize growth as a result of the tillage practices.

Table 4. Tillage operation and production costs for each tillage practice.

Tillage	Tillage cost ($·ha^{-1})	Production cost ($·ton^{-1})
CT	93.75 a	2.26 c
RT	17.24 b	4.32 b
ZT	*	5.25 a
P-value	0.0217	0.0380

Acknowledgements

This research was supported in part by funds administered through the Omar Al-Mukhtar University, Albida, Libya.

References

[1] Alldrissi, M., Sbeita, A., Jebriel, A., Zintani, A. and Shreidi, H. (1996) Libya: Country Report to the FAO International Technical Conference on Plant Genetic Resources. http://www.fao.org/fileadmin/templates/agphome/documents/PGR/SoW1/east/LIBYA.pdf

[2] Copeland, P.J. and Crookston, R.K. (1992) Crop Sequence Affects Nutrient Composition of Corn and Soybean Grown Under High Fertility. *Agronomy Journal*, **84**, 503-509. https://doi.org/10.2134/agronj1992.00021962008400030028x

[3] Riedell, W.E., Pikul, J.L., Jaradat, A.A. and Schumacher, T.E. (2009) Crop Rotation and Nitrogen Input Effects on Soil Fertility, Maize Mineral Nutrition, Yield, and Seed Composition. *Agronomy Journal*, **101**, 870-879. https://doi.org/10.2134/agronj2008.0186x

[4] Abagandura, O.G. and Park, D. (2016) Libyan Agriculture: A Review of Past Efforts, Current Challenges and Future Prospects. *Journal of Natural Sciences Research*, **6**, 57-67.

[5] Abagandura, O.G. (2016) Using Soil Conditioners to Improve Soil Physiochemical Properties and Agricultural Productivity in Libya. Ph.D. Thesis, Clemson University, SC, USA.

[6] Omar, S. (2017) pers. comm., 6 May. Employee in the Secretariat of Agriculture, Albida, Libya.

[7] Kausar, M.A., Chaudhry, F.M., Rashid, A., Latif, A. and Alam, S.M. (1976) Micronutrient Availability to Cereals from Calcareous Soils. *Plant Soil*, **45**, 397-410. https://doi.org/10.1007/BF00011702

[8] Strudley, M.W., Green, T.R. and Ascough, J.C. (2008) Tillage Effects on Soil Hydraulic Properties in Space and Time: State of the Science. *Soil Tillage Research*, **99**, 4-48. https://doi.org/10.1016/j.still.2008.01.007

[9] Schwen, A., Bodner, G., Scholl, P., Buchan, G.D. and Loiskandl, W. (2011) Temporal Dynamics of Soil Hydraulic Properties and the Water-Conducting Porosity under Different Tillage. *Soil Tillage Research*, **113**, 89-98. https://doi.org/10.1016/j.still.2011.02.005

[10] Costa, J.L., Aparicio, V. and Cerdà, A. (2015) Soil Physical Quality Changes under Different Management Systems after 10 Years in the Argentine Humid Pampa. *Solid Earth*, **6**, 361-371. https://doi.org/10.5194/se-6-361-2015

[11] Gómez, J.A., Giráldez, J.V., Pastor, M. and Fereres, E. (1999) Effects of Tillage Me-

thod on Soil Physical Properties, Infiltration and Yield in an Olive Orchard. *Soil and Tillage Research*, **52**, 167-175.

[12] Ji, B., Zhao, Y., Mu, X., Liu, K. and Li, C. (2013) Effects of Tillage on Soil Physical Properties and Root Growth of Maize in Loam and Clay in Central China. *Plant, Soil and Environment*, **59**, 295-302.

[13] Senjobi, B.A., Ande, O.T. and Okulaja, A.E. (2013) Effects of Tillage Practices on Soil Properties under Maize Cultivation on Oxic Paleustalf in South Western Nigeria. *Open Journal of Soil Science*, **3**, 163-168. https://doi.org/10.4236/ojss.2013.33019

[14] Shirani, H., Hajabbasi, M.A., Afyuni, M. and Hemmat, A. (2002) Effects of Farmyard Manure and Tillage Systems on Soil Physical Properties and Corn Yield in Central Iran. *Soil and Tillage Research*, **68**, 101-108.

[15] Lal, R. (1997) Long-Term Tillage and Maize Monoculture Effects on a Tropical Alfisol in Western Nigeria. I. Crop Yield and Soil Physical Properties. *Soil and Tillage Research*, **42**, 145-160.

[16] Sheldrick, B.H. and Wang, C. (1993) Particle Size Distribution. In: Carter, M.R. Ed., *Soil Sampling and Methods of Analysis*, Lewis Publications/CRC Press, Boca Raton, FL, 499-511.

[17] Nelson D.W. and Sommers L.E. (1982) Total Carbon, Organic Carbon, and Organic Matter. In: Page, A.L., *et al.*, Eds., *Methods and Soil Analysis*. *Part* 2. *Chemical and Microbial Properties*, Agronomy Monograph No. 9, 2nd Edition, ASA-SSSA, Madison, 539-557.

[18] Olsen S.R. and Sommers L.E. (1982) Phosphorus. In: Page, A.L., *et al.*, Eds., *Methods and Soil Analysis*. *Part* 2. *Chemical and Microbial Properties*, Agronomy Monograph No. 9, 2nd Edition, ASA-SSSA, Madison, 403-430.

[19] Miriti, J.M., Kironchi, G., Esilaba, A.O., Gachene, C.K.K., Heng, L.K. and Mwangi, D.M. (2013) The Effects of Tillage Systems on Soil Physical Properties and Water Conservation in a Sandy Loam Soil in Eastern Kenya. *Journal of Soil Science Environmental Management*, **4**, 146-154. https://doi.org/10.5897/JSSEM2013.0395

[20] Anderson, J.M. and Ingram, J.S.I. (1993) Tropical Soil Biology and Fertility. In: *A Handbook of Methods*, 2nd Edition, C.A.B. International, Wallingford, UK, 221.

[21] Bayhan, Y., Kayisoglu, B. and Gonulol, E. (2002) Effects of Soil Compaction on Sunflower Growth. *Soil and Tillage Research*, **68**, 31-38.

[22] Aikins, S.H.M., Afuakwa, J.J. and Owusu-Akuoko, O. (2012) Effect of Four Different Tillage Practices on Maize Performance under Rainfed Conditions. *Agriculture and Biology Journal of North America*, **1**, 1-51.

[23] Ben-Asher, J. and Silberbush, M. (1992) Root Distribution Under Trickle Irrigation: Factors Affecting Distribution and Comparison among Methods of Determination. *Journal of Plant Nutrition*, **15**, 783-794. https://doi.org/10.1080/01904169209364362

[24] Wang, X., Zhou, B., Sun, X., Yue, Y., Ma, W. and Zhao, M. (2015) Soil Tillage Management Affects Maize Grain Yield by Regulating Spatial Distribution Coordination of Roots, Soil Moisture and Nitrogen Status. *PLoS ONE*, **10**, e0129231.

[25] Ranjbarian, S., Mohammad, A. and Javad, J. (2015) Performance of Tractor and Tillage Implements in Clay Soil. *Journal of the Saudi Society of Agricultural Sciences*, **16**, 154-162.

[26] Archer, D.W., Pikul, J.L. and Riedell, W.E. (2002) Economic Risk, Returns and Input Use under Ridge and Conventional Tillage in the Northern Corn Belt, USA. *Soil and Tillage Research*, **67**, 1-8.

[27] Cassel, D.K. (1982) Tillage Effects on Soil Bulk Density and Mechanical Impedance.

In: Unger, P.W. and Van Doren, D.M., Eds., *Predicting Tillage Effects on Soil Physical Properties and Processes*, ASA and SSSA, Madison, WI, 45-67.

[28] Lampurlanés, J. and Cantero-Martinez, C. (2003) Soil Bulk Density and Penetration Resistance under Different Tillage and Crop Management Systems and Their Relationship with Barley Root Growth. *Agronomy Journal*, **95**, 526-536. https://doi.org/10.2134/agronj2003.0526

[29] Busari, M.A., Kukal, S.S., Kaur, A., Bhatt, R. and Dulazi, A.A. (2015) Conservation Tillage Impacts on Soil, Crop and the Environment. *International Soil and Water Conservation Research*, **3**, 119-129.

[30] Al-Hamed, S.A., Wahby, M.F. and Sayedahmed, A.A. (2016) Effect of Three Tillage Implements on Potato Yield and Water Use Efficiency. *American Journal of Experimental Agriculture*, **12**, 1-6. https://doi.org/10.9734/AJEA/2016/24950

[31] Wander, M.M. and Bollero, G.A. (1999) Soil Quality Assessment of Tillage Impacts in Illinois. *Soil Science Society of America Journal*, **63**, 961-971. https://doi.org/10.2136/sssaj1999.634961x

[32] Ferreras, L.A., Costa, J.L., Garcia, F.O. and Pecorari, C. (2000) Effect of No-Tillage on Some Soil Physical Properties of a Structural Degraded Petrocalcic Paleudoll of the Southern "Pampa" of Argentina. *Soil and Tillage Research*, **54**, 31-39.

[33] Fabrizzi, K.P., Garcıa, F.O., Costa, J.L. and Picone, L.I. (2005) Soil Water Dynamics, Physical Properties and Corn and Wheat Responses to Minimum and No-Tillage Systems in the Southern Pampas of Argentina. *Soil and Tillage Research*, **81**, 57-69.

[34] Singh, B. and Malhi, S.S. (2006) Response of Soil Physical Properties to Tillage and Residue Management on Two Soils in a Cool Temperate Environment. *Soil and Tillage Research*, **85**, 143-153.

[35] Alvarez, R. and Steinbach, H.S. (2009) A Review of the Effects of Tillage Systems on Some Soil Physical Properties, Water Content, Nitrate Availability and Crops Yield in the Argentine Pampas. *Soil and Tillage Research*, **104**, 1-15.

[36] Grant, C.A. and Lafond, G.P. (1993) The Effects of Tillage Systems and Crop Sequences on Soil Bulk Density and Penetration Resistance on a Clay Soil in Southern Saskatchewan. *Canadian Journal of Soil Science*, **73**, 223-232. https://doi.org/10.4141/cjss93-024

[37] Buschiazzo, D.E., Panigatti, J.L. and Unger, P.W. (1998) Tillage Effects on Soil Properties and Crop Production in The Subhumid and Semiarid Argentinean Pampas. *Soil and Tillage Research*, **49**, 105-116.

[38] Lin, H.S., McInnes, K.J., Wilding, L.P. and Hallmark, C.T. (1999) Effects of Soil Morphology on Hydraulic Properties: I. Quantification of Soil Morphology. *Soil Science Society of America Journal*, **63**, 948-954. https://doi.org/10.2136/sssaj1999.634948x

[39] Coquet, Y., Vachier, P. and Labat, C. (2005) Vertical Variation of Near-Saturated Hydraulic Conductivity in Three Soil Profiles. *Geoderma*, **126**, 181-191.

[40] Carof, M., De Tourdonnet, S., Coquet, Y., Hallaire, V. and Roger-Estrade, J. (2007) Hydraulic Conductivity and Porosity under Conventional and No-Tillage and the Effect of Three Species of Cover Crop in Northern France. *Soil Use and Management*, **23**, 230-237. https://doi.org/10.1111/j.1475-2743.2007.00085.x

[41] Smith, M.A., Carter, P.R. and Imholte, A.A. (1992) No-Till vs. Conventional Tillage for Late-Planted Corn Following Hay Harvest. *Journal of Production Agriculture*, **5**, 261-264. https://doi.org/10.2134/jpa1992.0261

[42] Lithourgidis, A.S., Tsatsarelis, C.A. and Dhima, K.V. (2005) Tillage Effects on Corn Emergence, Silage Yield, and Labor and Fuel Inputs in Double Cropping with

Wheat. *Crop Science*, **45**, 2523-2528. https://doi.org/10.2135/cropsci2005.0141

[43] Kayode, J. and Ademiluyi, B. (2004) Effect of Tillage Methods on Weed Control and Maize Performance in Southwestern Nigeria Location. *Journal of Sustainable Agriculture*, **23**, 39-45. https://doi.org/10.1300/J064v23n03_05

[44] Khurshid, K., Iqbal, M., Arif, M.S. and Nawaz, A. (2006) Effect of Tillage and Mulch on Soil Physical Properties and Growth of Maize. *American Journal of Agricultural and Biological Sciences*, **8**, 593-596.

[45] Liu, K. and Wiatrak, P. (2012) Corn Production Response to Tillage and Nitrogen Application in Dry-Land Environment. *Soil and Tillage Research*, **124**, 138-143.

[46] Diaz-Zorita, M. (2000) Effect of Deep-Tillage and Nitrogen Fertilization Interactions on Dryland Corn (*Zea mays* L.) Productivity. *Soil and Tillage Research*, **54**, 11-19.

[47] Videnović, Ž., Simić, M., Srdić, J. and Dumanović, Z. (2011) Long Term Effects of Different Soil Tillage Systems on Maize (*Zea mays* L.) Yields. *Plant, Soil and Environment*, **57**, 186-192.

[48] Shahid, M.N., Zamir, M.S.I., Haq, I.U., Khan, M.K., Hussain, M., Afzal, U. and Ali, I. (2016) Evaluating the Impact of Different Tillage Regimes and Nitrogen Levels on Yield and Yield Components of Maize (*Zea mays* L.). *American Journal of Plant Sciences*, **7**, 789-797. https://doi.org/10.4236/ajps.2016.76073

[49] Ion, V., Dicu, G., Dumbrava, M., Temocico, G., Alecu, I.N., Basa, A.G. and State, D. (2015) Harvest Index at Maize in Different Growing Conditions. *Romanian Biotechnological Letters*, **20**, 10951-10960.

[50] Reicosky, D.C. and Allmaras, R.R. (2003) Advances in Tillage Research in North American Cropping Systems. *Journal of Crop Production*, **8**, 75-125. https://doi.org/10.1300/J144v08n01_05

[51] Chauhan, B.S., Gill, G.S. and Preston, C. (2006) Tillage System Effects on Weed Ecology, Herbicide Activity and Persistence: A Review. *Animal Production Science*, **46**, 1557-1570. https://doi.org/10.1071/EA05291

Scientific Research Publishing

Open Journal of Soil Science, 2017, 7, 133-148
http://www.scirp.org/journal/ojss
ISSN Online: 2162-5379
ISSN Print: 2162-5360

Spatial Modeling of Soil Lime Requirements with Uncertainty Assessment Using Geostatistical Sequential Indicator Simulation

Jussara de Oliveira Ortiz[1], Carlos Alberto Felgueiras[1], Eduardo Celso Gerbi Camargo[1], Camilo Daleles Rennó[1], Manoel Jimenez Ortiz[2]

[1]INPE-Brazilian National Institute for Space Researches DPI-Divisão de Processamento de Imagens, São José dos Campos, Brazil
[2]Geopixel Soluções em Geotecnologias e TI, São José dos Campos, Brazil
Email: jussara@dpi.inpe.br, carlos@dpi.inpe.br, camilo@dpi.inpe.br, eduardo@dpi.inpe.br, manoel.ortiz@geopixel.com.br

How to cite this paper: de Ortiz, J.O., Felgueiras, C.A., Camargo, E.C.G., Rennó, C.D. and Ortiz, M.J. (2017) Spatial Modeling of Soil Lime Requirements with Uncertainty Assessment Using Geostatistical Sequential Indicator Simulation. *Open Journal of Soil Science*, **7**, 133-148.
https://doi.org/10.4236/ojss.2017.77011

Received: April 10, 2017
Accepted: July 10, 2017
Published: July 13, 2017

Abstract

This work presents and analyses a geostatistical methodology for spatial modelling of Soil Lime Requirements (*SLR*) considering punctual samples of Cation Exchange Capacity (*CEC*) and Base Saturation (*BS*) soil properties. Geostatistical Sequential Indicator Simulation is used to draw realizations from the joint uncertainty distributions of the *CEC* and the *BS* input variables. The joint distributions are accomplished applying the Principal Component Analyses (*PCA*) approach. The Monte Carlo method for handling error propagations is used to obtain realization values of the *SLR* model which are considered to compute and store statistics from the output uncertainty model. From these statistics, it is obtained predictions and uncertainty maps that represent the spatial variation of the output variable and the propagated uncertainty respectively. Therefore, the prediction map of the output model is qualified with uncertainty information that should be used on decision making activities related to the planning and management of environmental phenomena. The proposed methodology for *SLR* modelling presented in this article is illustrated using *CEC* and *BS* input sample sets obtained in a farm located in Ponta Grossa city, Paraná state, Brazil.

Keywords

Spatial Modeling of Soil Attributes, Indicator Geostatistics, Joint Simulation, Principal Component Analyses, Spatial Uncertainty Analyses

1. Introduction

Soil acidity is one of the factors that limits crop yields in various places of the world. Brazilian soils are mostly acids, mainly for the tropical Savanna regions,

known in Brazil as Cerrado. Such soils are characterized by low concentrations of calcium and magnesium, elements directly involved in the development of the plant [1].

The appropriate correction of soil acidity, or liming, is considered an effective practice for the use of soil nutrients by plants [2], which promoting increased soil fertility and hence productivity. For this purpose, the limestone is an agricultural input with efficient response to correct soil acidity. It is relatively cheap in Brazil and it is of simple application. The literature shows a limestone relation to the increase in production, involving the raising of productivity of grain crops, mainly soybeans, wheat and corn, with proper fertilization, or replacement of nutrients in the soil [3] [4] [5] [6].

However, any application of high or insufficient doses of inputs in the soil will reflect in plant nutrition so that, if not corrected by cover fertilizations, will increase or decrease the productivity. Therefore, the recommendation of the amount of limestone, like any other fertilizer, must comply with a soil analysis, which should avoid unnecessary applications that would lead to super liming. According to some authors [7] [8], super liming would be as damaging as high acidity and it would be difficult to correct.

To obtain higher yields and to apply inputs in the soil with no waste, there is a tendency to use methods of input estimates based on spatial variability of soil properties. These estimates lead to application of inputs, by variable rates in the geographic space, with the purpose of optimizing profit, productivity and environmental sustainability. These practices, known as Precision Agriculture (PA), implement the process of agricultural automation, dosing fertilizers and pesticides for the soil of a geographical area of interest. This set of agriculture tools involves the use of Geodesic Positioning Systems (GPS), Geographic Information Systems (GIS) with integrated statistics methods, and instruments with sensors for measurement or detection of parameters on targets of interest in the agroecosystem (soil, plant, insects and diseases).

Several authors have adopted the geostatistical procedures in PA to estimate and evaluate the spatial variability of soil properties [9] [10] [11] [12] [13]. Specifically, indicator geostatistical procedures have been widely used because they are non-parametric methods, *i.e.*, they do not require the definition of a priori probability model [14] [15] [16]. In addition, predictions maps (mean, median or mode value), and uncertainty maps (based on deviation values or probability of default quantiles) are extracted by inference and simulation methods. So, the predictions are accompanied with their respective uncertainties, which are also spatially distributed in the study area. Take into account the uncertainty information during the modeling process is important, because it allows to qualify the result of the used model, which should be considering for planning and decision making related to the investigated properties [17] [18] [19].

In this context, this work applies and analyses indicator geostatistical procedures for spatial modelling of Soil Lime Requirements (*SLR*), derived from a model proposed by [20]. The *SLR* model is based on the relationship between

Cation Exchange Capacity (*CEC*) and Base Saturation (*BS*) properties. These soil chemical properties affect soil acidity, and subsequently soil fertility and yield. So, the idea of the *SLR* modelling is to show the soil regions that need correction, raising the saturation of the bases to a value that provides maximum economic efficiency of the limestone application.

This work is organized in 6 sections. Besides the Section 1, presenting the introduction, the Section 2 addresses the main necessary theoretical concepts. Section 3 synthesizes the proposed methodology. The Section 4 explores a case study of *SLR* modeling with real data. Section 5 presents the results, followed of analyses and discussions. Finally, the Section 6 reports important conclusions with suggestions for future works involving research aspects of this work.

2. Concepts

2.1. The Spatial SLR Model

Liming depends on the decision to apply or not the limestone and the definition of its quantities, if it is required. This is done through some formulated mathematically methods and they are related to the soil characteristics of each geographic region.

Among the several methods for liming recommendation, the base saturation method, presented by [20] was defined as the most suitable for the study region. It is based on the relationship between *BS* and *CEC*. The model parameters are considered for the soil, soil amendment and the crop. The method consists in raising the saturation of the bases to a value that provides maximum economic efficiency of the of limestone application.

The neutralizing power, the granulometry and reactivity of the limestone are important factors for the correct choice of it. The neutralizing power is determined by comparison with the power of neutralization of pure calcium carbonate ($CaCO_3$), with the maximum value equal 100. For this reason, it is called the Relative Power of Total Neutralization (*RPTN*) or calcium carbonate equivalent, and the knowledge of this parameter is relevant to determine the *SLR*. The model to determine *SLR*, in tons/hectare (t/ha), according to recommendations about soils presented in [6] is expressed as:

$$SLR(\boldsymbol{u}) = \frac{\left(BS_2 - BS_1(\boldsymbol{u})\right) \cdot CEC(\boldsymbol{u})}{RPTN} \tag{1}$$

where: $\boldsymbol{u}$ is a vector of the geographic coordinates where the input variables are sampled inside of the study area; $BS_1(\boldsymbol{u})$ is the base saturation value of the original soil, given in percentage, before correction. They are sampled directly from the ground, analyzed in the laboratory and should be elevated to the level considered suitable for the crop and soil studied; BS_2 is the base saturation value that you want to achieve; there is a default value for each crop; $CEC(\boldsymbol{u})$ is the sum of the bases with the values of potential acidity; *RPTN:* is the Relative Power of the Total Neutralization in relation to the limestone adopted and it is, generally, less than 100 (the total neutralization).

According to [21] the BS_2 is variable for each State or region and, as defined before, at Parana State this value is 70% and *RPTN* is the Relative Power of the Total Neutralization in relation to the limestone adopted and it is, generally, less than 100%, that is the total neutralization; The limestone that has been used at the study farm presents a *RPTN* equivalent to 85%. So, the model to calculate Limestone Requirement is:

$$SLR(\boldsymbol{u}) = \frac{(70 - BS(\boldsymbol{u})) * CEC(\boldsymbol{u})}{850} \tag{2}$$

The spatial modeling applied to the investigation of a phenomenon of interest requires mathematical models that work on estimate values of the input variables and their uncertainties. The output estimates only depend on the input variables while the output uncertainties are propagated from the uncertainties of the input variables. The output uncertainties are used to qualify the spatial model output. Knowing the quality of the model results is important, especially when they are used in decision making activities associated to the planning and management of the investigated phenomena [22].

When management planning requires local estimates and mathematical models are considered, the uncertainty propagated in the predictions might be evaluated. Knowing the quality of the model results is fundamental, especially when they are used in spatial decision making [22], with GIS operations.

Some uncertainty propagation techniques were presented by [23]. The first order Taylor series and the Monte Carlo simulation can be stand out.

The Monte Carlo simulations were considered in this work. Let $U(.)$ be the output of a GIS operation $g(.)$ on m input attributes $A_i(.): U(.) = g(A_1,(.),\cdots,A_m(.))$. The idea of the method is to compute the result on $g(a_1,\cdots,a_m)$ repeatedly, with input values a_i that are randomly sampled from their joint distribution.

Application of the Monte Carlo method to uncertainty propagation with non-point operations requires the simultaneous generation of realizations from $A_i(.)$. This implies that spatial correlation will have to be accounted for. The technique adopted in this paper for stochastic spatial simulation, was the joint sequential Indicator simulation algorithm [14] with principal component analysis, as presented in the next item.

The idea of the Taylor series method is to approximate $g(.)$ by a truncated Taylor series centred at $\bar{b} = (b_1,\cdots,b_m)$ [23].

The first order Taylor series of $g(.)$ around $\bar{b}$ is given by:

$$U = g(\bar{b}) + \sum (A_i - b_i) g_i'(\bar{b}) \tag{3}$$

where $g_i'(.)$ is the first derivative of $g(.)$ with respect to its i-th argument. The variance σ^2 is given as:

$$\sigma^2 = \sum\sum \rho_{ij}\sigma_i\sigma_j g_i'(\bar{b}) g_j'(\bar{b}) \tag{4}$$

where: σ_i *and* σ_j are the standard deviation of the *i* and *j* variables respectively and ρ_{ij} *is* the correlation between them.

As the *SLR* model considers only two variables, the Equation (4) will be as bellow:

$$\sigma^2 = \sum_{i=1}^{2}\sum_{j=1}^{2}\rho_{ij}\sigma_i\sigma_j g_i'(\bar{b})g_j'(\bar{b}) \tag{5}$$

i represents the variable *BS* and *j* represents the variable *CEC.*

And when Equation (5) is applied on the model as,

$$g = SLR = \frac{(70 - BS) * CEC}{850} \tag{6}$$

the derivatives are as bellow:

$$\frac{\partial g}{\partial BS} = \frac{-CEC}{850} \quad \text{and} \quad \frac{\partial g}{\partial CEC} = \frac{70 - BS}{850} \tag{7}$$

2.2. Principal Component Transformation

Many spatial models that make use of the several input variables required the determination of joint probability distributions of these variables for generation of the new information and for uncertainty evaluation, that usually are built via simulation methods.

When the input variables are correlated, their distributions should not be simulated independently. The direct approach is to use a joint simulation of the dependent variables, but it requires the inference and modeling of direct and cross covariance matrices that are computational costly to determine [14].

An alternative mode is first to decorrelate the input variables using Principal Component Analysis-*PCA* [24] [25] and, after apply the geostatistical simulation procedure. So, the *M* interdependent input variables, denoted by $Z_M(\boldsymbol{u}) = \{Z_1(\boldsymbol{u}), Z_2(\boldsymbol{u}), \cdots, Z_m(\boldsymbol{u})\}$, $m = 1, \cdots, M$, are transformed in *M* independent variables, denoted by $Y_M(\boldsymbol{u}) = \{Y_1(\boldsymbol{u}), Y_2(\boldsymbol{u}), \cdots, Y_m(\boldsymbol{u})\}$, as follows:

$$Y_M(\boldsymbol{u}) = \varphi(Z_M(\boldsymbol{u})) \tag{8}$$

where φ is the transformation function of the *PCA*.

To recover the interdependent variables $Z_M(\boldsymbol{u})$ applies the inverse transform function, as follows:

$$Z_M(\boldsymbol{u}) = \varphi^{-1}(Y_M(\boldsymbol{u})) \tag{9}$$

where φ^{-1} is the inverse transformation of the *PCA*.

2.3. Indicator Geostatistical Approach

The indicator geostatistical approach for continuous variables, for example for the $Y_M(\boldsymbol{u})$ variables, allows to estimate a set of values at non sampled location, that represent a discretized approximation of the conditional cumulative distribution function (*ccdf*) [15] [26].

Initially the variables $Y_M(\boldsymbol{u})$ are transformed into indicator variables, considering y_M^c cutoffs values, $c = 1, \cdots, n$ *cutoffs*. These transformations are defined by the relation:

$$I_M(\boldsymbol{u}; y_M^c) = \begin{cases} 1 & \text{se } Y_M(\boldsymbol{u}) \le y_M^c \\ 0 & \text{se } Y_M(\boldsymbol{u}) > y_M^c \end{cases} \tag{10}$$

The transformation expressed in Equation (8) is equivalent to associate probability 1 (100%) for $Y_M(\boldsymbol{u})$ values which are smaller than or equal to the cutoff y_M^c and 0 otherwise. So, for each cutoff value indicator fields are generated, with 0 and 1 values, of the indicator variable $I_M(\boldsymbol{u}; y_M^c)$.

Next, empirical indicator semivariograms are determined for each one of the indicator fields to estimated their spatial correlation structures:

$$\hat{\gamma}_M(\boldsymbol{h}, y_M^c) = \frac{1}{2N(\boldsymbol{h})} \sum_{j=1}^{N(\boldsymbol{h})} \left[i(\boldsymbol{u}; y_M^c) - i(\boldsymbol{u}+\boldsymbol{h}; y_M^c) \right]^2 \tag{11}$$

where $i(\boldsymbol{u}; y_M^c)$ and $i(\boldsymbol{u}+\boldsymbol{h}; y_M^c)$ are values of the indicator variable $I_M(\boldsymbol{u}; y_M^c)$ separated by the distance vector $\boldsymbol{h}$, and $N(\boldsymbol{h})$ is the number of the pairs points that are separated by the distance vector $\boldsymbol{h}$.

The indicator fields associated with their respective cutoff values and theoretical semivariograms are used by Indicator Kriging (*IK*) and Conditional Sequential Indicator Simulation (*SIS*) procedures for estimating probabilities values at non-sampled location. Thus, this set of estimated probabilities, at non sampled location, is used to create a discretized approximation of the *ccdf* [15] [27]) and it represents the uncertainty model of the variable.

2.4. Conditional Sequential Indicator Simulation

A stochastic simulation is a process of drawing equally likely realizations of values that are obtained from the probability distribution of a Random Variable (RV).

Consider the M independent factors $Y_M(\boldsymbol{u})$. Then, a set of the realizations equally likely are generated by geostatistical simulation, denoted by $Y_M^L(\boldsymbol{u}_\alpha)$, where L is the simulation number; $\boldsymbol{u}_\alpha$ = 1, ···, gridsize (nlines x ncolumns), are locations regularly distributed in the geographic space, determining a regular grid representation structure. For example, to the $Y_2(\boldsymbol{u})$ independent variable, $Y_2^L(\boldsymbol{u}_\alpha) = \{y_2^l(\boldsymbol{u}_\alpha)\}$, where $l = 1, \cdots, L$; $y_2^l(\boldsymbol{u}_\alpha)$ is the l-th simulated value at $\boldsymbol{u}_\alpha$; and the set $\{y_2^l(\mathbf{u}_\alpha)\}$ represent the l-th random field generated by simulation of the $Y_2(\boldsymbol{u})$. In that case, the SIS procedures makes use of the *ccdf*, conditioned to the n nearest of RV $Y_2(\boldsymbol{u})$ and also to the pre-simulated values, inside the $\boldsymbol{u}_\alpha$ neighborhood, to get $y_2^l(\boldsymbol{u}_\alpha)$ values.

The *SIS* procedure has the following steps [15]:

1) Sets up randomly one $\boldsymbol{u}_\alpha$ location. Then simulates a value of the $y_2^l(\boldsymbol{u}_\alpha)$ from the univariate *ccdf* of $Y_2(\boldsymbol{u}_\alpha)$, $\text{Prob}\left[Y_2(\boldsymbol{u}_\alpha) \le y_2(\boldsymbol{u}_\alpha) \mid n\right]$, conditioned to the n nearest sample data $Y_2(\boldsymbol{u})$;

2) Once simulated, $y_2^l(\boldsymbol{u}_\alpha)$ becomes a conditioning data for subsequent simulation steps. The conditioning data is updated to $(n+1) = (n) \cup \{Y_2(\boldsymbol{u}) = y_2^l(\boldsymbol{u}_\alpha)\}$;

3) Sets up randomly another location $\boldsymbol{u}'_\alpha \neq \boldsymbol{u}_\alpha$. Simulated a new value of the $y_2^l(\boldsymbol{u}'_\alpha)$ from the univariate *ccdf* of $Y_2(\boldsymbol{u}'_\alpha)$, $\text{Prob}\left[Y_2(\boldsymbol{u}'_\alpha) \le y_2(\boldsymbol{u}'_\alpha) \mid (n+1)\right]$, conditioned to the information set $(n+1)$;

4) Update the information set $(n+1)$ to a new information set $(n+2) = (n+1) \cup \{Y_2(\boldsymbol{u}) = y_2(\boldsymbol{u}'_\alpha)\}$;

5) Repeat the two previous steps until all the locations $\boldsymbol{u}_\alpha$ of the spatial grid have been simulated. At this time was produced a random field of the $Y_2(\boldsymbol{u})$;

6) Repeat all steps for generating new random fields of the $Y_2(\boldsymbol{u})$. Stop when you reach the desired number of simulations.

3. Methodology

The proposed methodology for *SLR* modelling is illustrated in the Figure 1, using $BS(\boldsymbol{u})$ and $CEC(\boldsymbol{u})$ input sample sets obtained in a farm located in Ponta Grossa city of Paraná State, Brazil. The variables $BS(\boldsymbol{u})$ and $CEC(\boldsymbol{u})$, hereafter

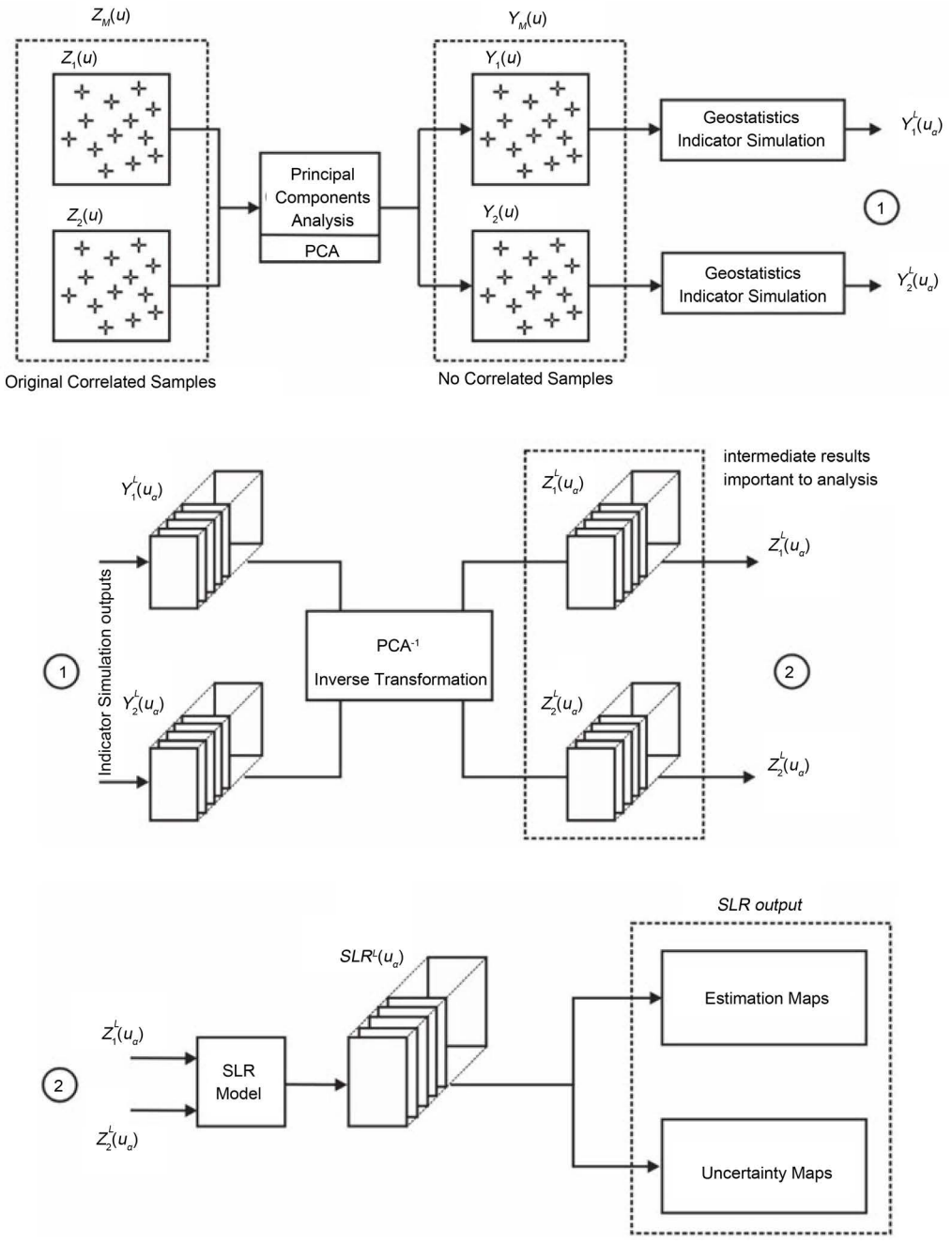

Figure 1. Methodological sequence applied to $CEC(\boldsymbol{u})$ and $BS(\boldsymbol{u})$ soil attributes to model *SLR*.

are named in this Section as $Z_1(\boldsymbol{u})$ and $Z_2(\boldsymbol{u})$, respectively.

Initially, the input variables $Z_1(\boldsymbol{u})$ and $Z_2(\boldsymbol{u})$ are decorrelated via *PCA* transformation in order to get two uncorrelated sample sets named $Y_1(\boldsymbol{u})$ and $Y_2(\boldsymbol{u})$ variables. Following, $Y_1(\boldsymbol{u})$ and $Y_2(\boldsymbol{u})$ are independently spatialized applying SIS procedure. The result is a set of the realizations equally likely, $Y_1^L(\boldsymbol{u}_\alpha)$ and $Y_2^L(\boldsymbol{u}_\alpha)$. Since the simulation values were obtained from the independent variables distributions [$Y_1(\boldsymbol{u})$ and $Y_2(\boldsymbol{u})$], it is necessary to apply to them PCA^{-1}, the inverse transformation of *PCA*, in order to obtain a set of dependent realizations, $Z_1^L(\boldsymbol{u}_\alpha)$ and $Z_2^L(\boldsymbol{u}_\alpha)$. From theses realizations, prediction and uncertainty maps can be generated. These maps are intermediate results that help the analyst to better understand the spatial distribution of the variables involved in the *SLR* model and their respective uncertainties. So, the simulated fields $Z_1^L(\boldsymbol{u}_\alpha)$ and $Z_2^L(\boldsymbol{u}_\alpha)$ are selected randomly several times, via Monte Carlo method and after applied in the spatial *SLR* model. From the resulting SLR fields, prediction and uncertainty maps are generated. These maps represent the spatial variation of the output variable and the propagated uncertainty, respectively. Therefore, the prediction map generated by spatial *SRL* model is qualified with uncertainty information

Given a spatial region of interest, the methodology applied has the following steps:

1) In a set of spatial correlated sample points of the *CEC* and *BS* soil attributes, hereafter named in this text Z_1 and Z_2 variables, apply the *PCA* transformation in order to get two uncorrelated variables Y_1 and Y_2;

2) Apply the indicator sequential simulation on the Y_1 and Y_2 variables in order to get independent grids representing fields of draw values of these variables;

3) The draw values of Y_1 and Y_2 are back transformed using a PCA^{-1} approach resulting on a set of dependent grids representing fields of draw values of the Z_1 and Z_2 variables;

4) Extract statistic properties of the *CEC* and *BS* draw values: prediction maps of mean or median values, for example, and uncertainty maps based in confidence interval of standard deviations or quantiles. This is important to observe the individual spatial distribution of the estimated and uncertainty values of the input variables;

5) Obtain draw values, randomly chosen, from the *SLR* model applied to the dependent draw values of the Z_1 and Z_2 variables;

6) Extract statistic properties of the *SLR* draw values: prediction maps of mean or median values, for example, and uncertainty maps based in confidence interval of standard deviations or quantiles.

In this article the final resulting maps of predictions and uncertainties are analyzed and. Figure 1 illustrates the applied methodology.

4. A Case Study

4.1. The Study Area and Input Data

The study region, Figueira farm, is located in the city of Carambeí, PR, Brazil,

and comprises an area of 392 ha. The farm has been adopted a precision agriculture system and the main cultures are soy, wheat and corn. In order to illustrate the methodology of this work, it was used as information a set of points of soil chemical properties (*BS* and *CEC*). These data were sampled at field by a Brazilian company that works with precision agriculture [28]. The geographical positioning of the samples was gathered by Global Positioning System, GPS, which ensures accurate georeferencing, as shown in the Figure 2.

5. Results and Discussion

The results presented below were obtained from simulated fields of input variables of *CEC* and *BS*. These fields were produced using specific functions from geostatistical software called GSLIB [14]. As mentioned before the soil attributes, *CEC* and *BS* are interdependent and the correct spatial modeling requires the joint simulation of these variables.

In this study an alternative to joint simulation was implemented, and it was possible to simulate separately a set of independent factors from which the original variables can be reconstituted [14] [15]. The factors were obtained from Principal Component Analysis and the interdependence was guaranteed by the common inverse transform. The indicator simulation was performed over the

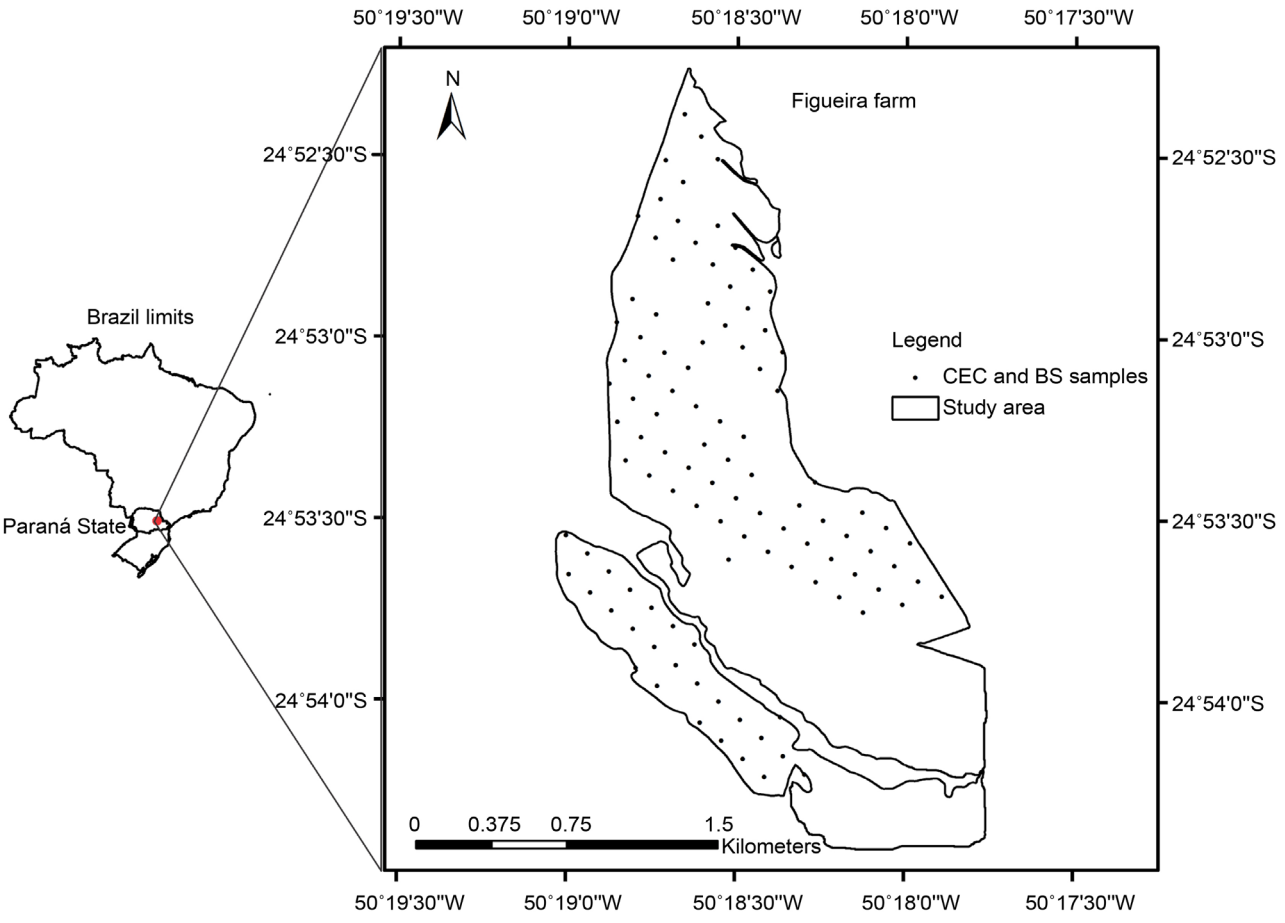

Figure 2. Study area Figueira farm in Paraná state.

independent sample set and simulated fields were generated. These independent simulated fields were back transformed into simulated values/fields for the original variables and they represent their stochastic uncertainty models.

In this case study, for each input variable, the number of realizations was fixed to 400 and they were represented in regular grid structures with 200 lines by 200 columns. That number of runs is considered sufficiently large to reach high accuracies. From those simulated values it could be generated the prediction and uncertainties maps. Thus, the mean estimates map was calculated by arithmetic average of the simulated values at each spatial position. Similarly, an uncertainty map was based on calculating the standard deviation of those same simulated values.

The resulting data were organized in a geographic database using the GIS SPRING [29]. This GIS enabled the visualization of spatial input information and the results of the spatial model explored.

Figure 3 shows the predicted values, grid of mean values, obtained from the uncertainty models of *CEC* and *BS* soil properties. From these maps that represent the outline of the study area, it can be observed the spatial distribution of each attribute, along with their minimum and maximum values.

Figure 4 depicts the uncertainty maps with confidence intervals based on standard deviation values of the uncertainty models of CEC and BS soil properties.

The maps of the Figure 4 indicate that the highest uncertainties, red areas, appear in regions where higher local variations of the predicted values occur. This is an expected result since the uncertainties of the indicator simulation approach are proportional to the local density of the samples and to their local value variations. These maps represent the spatial distribution of the uncertainties where one can get, for instance, the general idea of the areas with the most

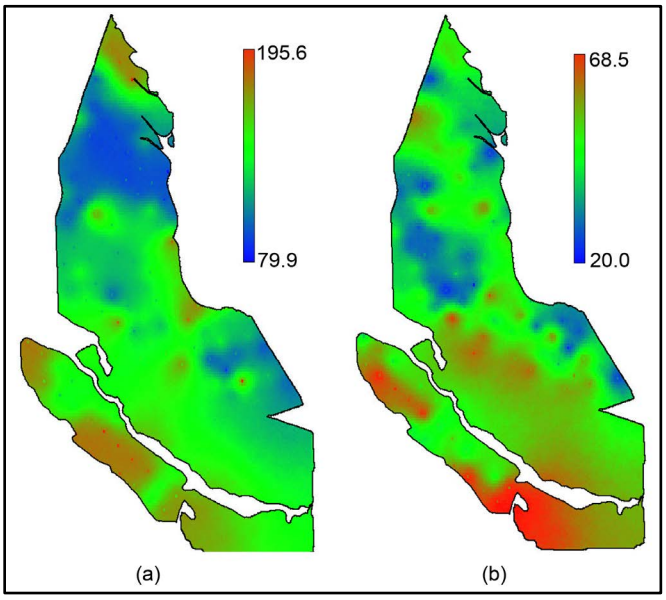

Figure 3. Map of predicted mean values from simulated fields of (a) *CEC* and (b) *BS*.

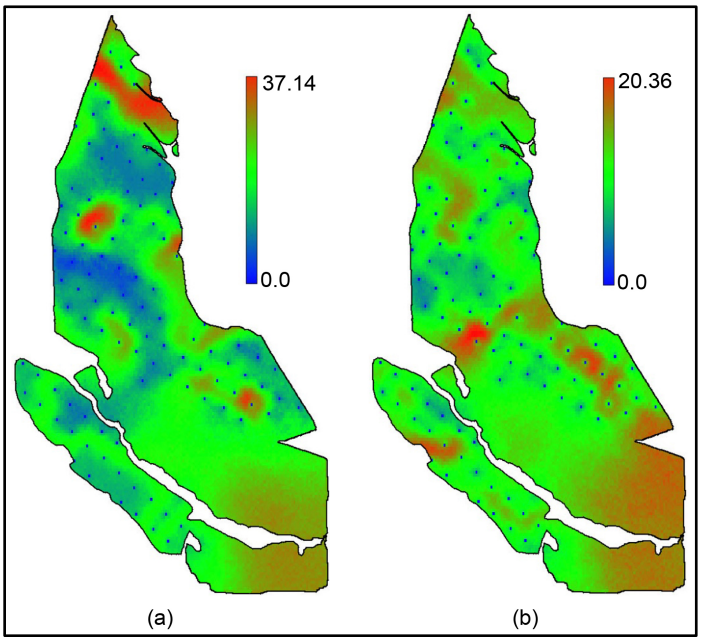

Figure 4. Map of uncertainty values, based on standard deviation confidence intervals, from simulated fields of (a) *CEC* and (b) *BS* soil properties.

reliable estimates. These uncertainty values are propagated to the resulting uncertainty maps of any spatial modelling that integrate these variables.

6. Modeling Results and Uncertainty Propagation

In the Figueira Farm the correction of soil acidity was modeled by estimating soil lime requirement, as a function of the *CEC* and *BS* that are the input variables of the model, *SLR*, presented in Equation (2). Those variables were simulated previously (**Figure 3**) and their uncertainty values (**Figure 4**) will propagate through these model, leading to uncertain response values of the *SLR*. **Figure 5** presents the predicted and uncertain maps resulting of the *SLR* spatial modelling. These maps were generated from the application of the Monte Carlo approach on the back transformed fields, or the correlated simulated fields, of the *CEC* and *BS* variables. In this procedure 400 fields were generated from the final model obtained by applying Equation (2) in the simulated values of the input variables, randomly drawn. The simulated values from those fields, at each spatial location, were used to generate the maps presented in the **Figure 5(a)**, mean of *SLR* and **Figure 5(b)** standard deviation of the *SLR*.

In the **Figure 5(a)** the map of means presents the spatial distribution of the mean values estimated of the *SLR*. That map shows that regions with high *SLR* values, in red, are those in which the *CEC* values are higher and *BS* is lower. The map of standard deviation, **Figure 5(b)**, shows the spatial distribution of the uncertainty values propagated to final modeling result. As expected, at this uncertainty map are observed high uncertainty areas in red, where there is a greater spatial variability in the values inferred by the model.

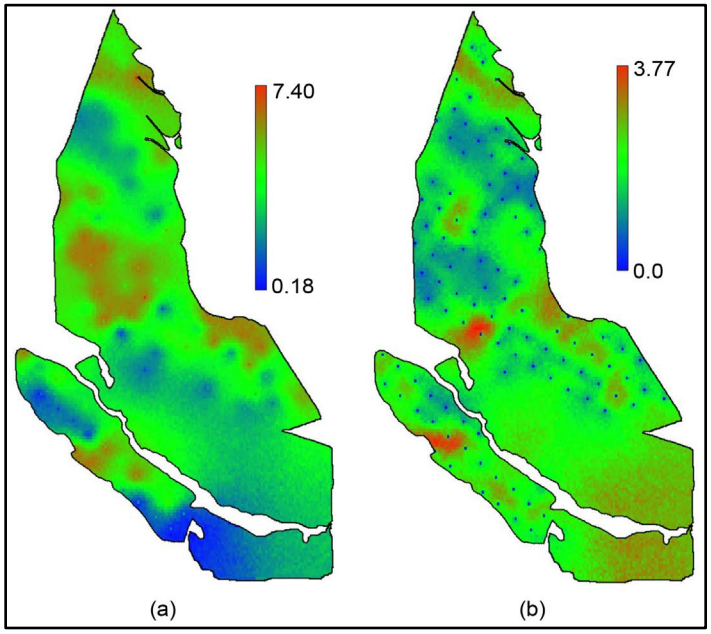

Figure 5. SLR results of (a) predicted mean (b) uncertainty values from joint simulation process.

7. Discussion

Figure 6(a) presents uncertainty map resulting from the *SLR* spatial modelling regarding to correlation between the variables *CEC* and *BS* to perform the joint simulation, and **Figure 6(b)** shows the uncertainty map considering independence between them. The maps are plotted in a same color scale (0 to 6.44) in order to be compared. Comparing the uncertainty maps of **Figure 6**, it can be observed that the uncertainty gets smaller for the *SLR* results when the correlation between the input variables is considered. In this case this correlation is positive and the final propagated result of the *SLR* model agrees with the concepts explained in the Section 2.5.

When the Taylor expression (Equation (6)) is applied on the model SLR (Equation (2)), replacing the first derivatives as presented in Equation (7), it is possible to evaluate that as higher correlation between the input variables as lower the uncertainty propagation in the final results. So this information can be associated with the results analysis.

Although most users are aware with uncertainty in GIS operations, they have not paid attention to the problem of correlated variables in spatial modelling. To emphasize this important issue we have considered three different correlations levels, including the measured, to apply the Taylor series: one of them is higher than the original measured correlation $\rho = 0.8$; the true correlation of the data, $\rho = 0.51$ and a lower correlation $\rho = 0.2$. The results, presented in the **Figure 7**, show that the propagated uncertainty decreased when the correlation increased.

The uncertainty maps are used to qualify the inferences. So, in decision-making processes, it can be considered just uncertainties values above or below of a settled threshold, giving priority to areas that are best suited to the problem that is

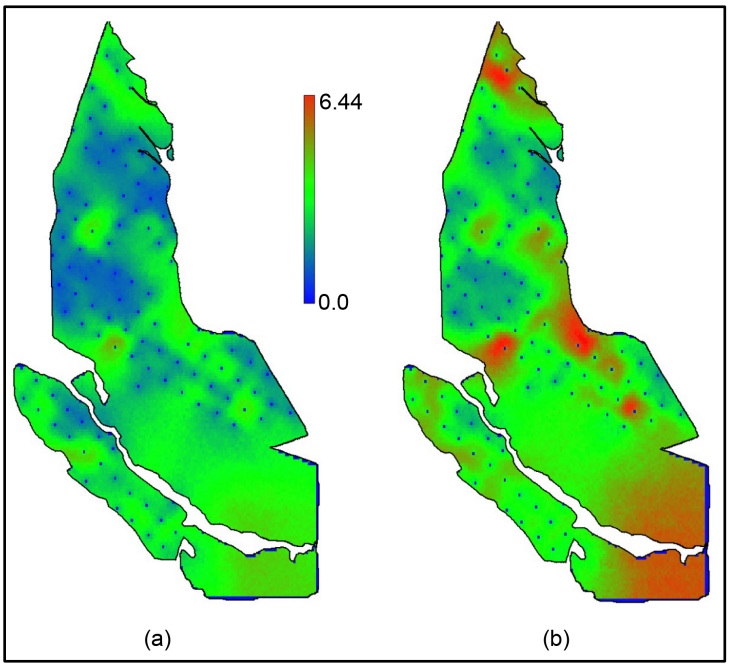

Figure 6. Uncertainty maps: (a) Joint simulation; (b) Independence between CEC and *BS*.

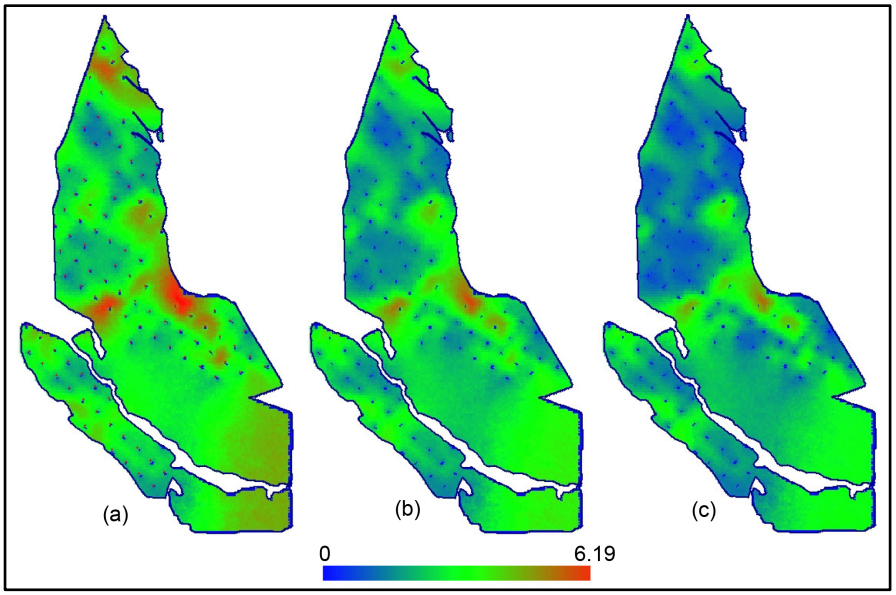

Figure 7. Uncertainty maps with Taylor series: (a) Correlation 0.8; (b) Correlation 0.5; and (c) Correlation 0.2.

being addressed. In this work, which is modeling the need for limestone, the decision maker can evaluate the available resources and define important thresholds, upper and lower, for the implementation of necessary agricultural inputs. It is important to consider that the excess of limestone can be as or more harmful than the lack of it for a particular crop. So, incorporate uncertainty maps to a precision farming system adds quality to the agricultural planning that requires information with spatial representation.

8. Conclusions

In order to make good decisions in precision agriculture, considering a field with acid soil, as this study case, the determination of the best liming practice depends on the uncertainty analysis. Spatial modelling as presented in this paper has to consider the level of uncertainty about the input parameters of the model, soil properties, and their propagation. Specifically, when those parameters are correlated their distributions cannot be sampled independently. So, this study was concerned about it and replaces the joint distribution to the principal component analysis.

In this work, we used the geostatistical simulation procedure for nomination to represent soil properties that are correlated. Applied an approach based on the analysis of principal components to obtain the achievements, with dependencies, these simulations. These achievements have been integrated via Monte Carlo method to obtain limestone need values according to a predefined spatial model.

The methodology for modeling the liming requirements was proved easy to implement and the results showed consistency with the spatial model and its input variables. In this modeling were obtained, besides the prediction maps, maps the uncertainties of the input variables and the final model that reflects the propagated uncertainty. He showed up at work, the propagated uncertainty is overrated if you do not consider different correlations of zero between model input variables. It is able to highlight areas with higher lime requirements and it is possible to identify areas with higher uncertainties in relation to the predictions. With those results the decision maker can, for instance, choose the first areas candidate for liming if there are financial problems. To reduce uncertainties is a very important point to policy makers who, many times, have to decide and to assess the consequences of different decisions, even decide for no action if the uncertainties are big.

Acknowledgements

The authors would like to thank FAPESP the São Paulo Research Foundation for the support obtained, via process number 2015/24676-9, to develop the researches that allows the realization of this article.

References

[1] Pitta, G.V., Coelho, A.M., Alves, V.M.C., França, G.E. and Magalhães, J.V. (2006) Cultivo Do Milho. Embrapa Sorgo E Milho, versão eletrônica, Dez. https://www.infoteca.cnptia.embrapa.br/infoteca/bitstream/doc/487015/1/Com53.pdf

[2] Caires, E.F., Garbuio, F.J., Churka, S., Barth, G. and Correa, J.C.L. (2008) Effects of Soil Acidity Amelioration by Surface Liming on No Till Corn, Soybean And Wheat Root Growth and Yield. *European Journal of Agronomy*, **28**, 57-64. https://doi.org/10.1016/j.eja.2007.05.002

[3] Anderson, N.P., Hart, J.M., Sullivan, D.M., Christensen, N.W., Hornek, D.A. and Pirelli, G.J. (2013) Applying Lime to Raise Soil pH for Crop Production, Oregon State University. Extension Publication FG52, Corvallis, Oregon.

https://catalog.extension.orenstate.edu/em9057

[4] Mallarino, A., Pagani, A. and Sawyer, J.E. (2011) Corn and Soybean Response to Soil pH Level and Liming. *Integrated Crop Management Conference*, Ames, Iowa, 30 November-1 December 2011, 93-102.

[5] Korndorfer, G.H., Pereira, H.S. and Camargo, M.S. (2004) Silicatos De Cálcio E Magnésio Na Agricultura. 3rd Edition, GPSi/ICIAG/UFU, Technical Report, Uberlândia, 28 p.

[6] Fukuda, C. and Otsubo, A.A. (2003) Cultivos na Região Centro Sul do Brasil. Embrapa Solos, Sistema de Produção, Eletronic Version. http://www.embrapa.br

[7] Padua, T., de Padua, P., Silva, C. and de Oliveira Dias, B. (2008) Nutrição E Crescimento Do Algodoeiro Em Latossolo Sob Diferentes Coberturas Vegetais E Manejo De Calagem. *Ciência e Agrotecnologia*, **32**, 1481-1490. https://doi.org/10.1590/S1413-70542008000500019

[8] Silva, P.A., Rigato, L.I., Jales, de Lima Jales, L., Polessa, M.F., Sather, M., Neto, R.B., Passos, J.L., de Souza, C.M., dos Santos, J.N.B. and do Amaral, J.A.T. (2013) Estudo Mineral De Uma Super Calagem No Milho. CCA-UFES/Fitotecnia, Alto universitário, Alegre, ES. http://biblioteca.univap.br/dados/INIC/cd/inic/IC5%20anais/IC5-13.PDF

[9] Vettorazzi, C.A. and Ferraz, S.F.B. (2000) Silvicultura De Precisão: Uma Nova Perspectiva Para O Gerenciamento De Atividades Florestais. In: Borém, A., Giudice, M.P., de Queiróz, D.M., *et al*., Eds., *Agricultura De Precisão*, Os Autores, Viçosa, 65-75.

[10] Ortiz, J.L. (2003) Emprego Do Geoprocessamento No Estudo Da Relação Entre Potencial Produtivo De Um Povoamento De Eucalipto E Atributos Do Solo E Do Relevo. Dissertação (Mestre em Recursos Florestais), ESALQ/USP, Piracicaba, SP.

[11] Oliver, M.A. (2013) Precision Agriculture and Geostatistics: How to Manage Agriculture More Exactly. *The Royal Statistical Society*, **10**, 17-22.

[12] Krasilnikov, P., Carré, F. and Montanarella, L. (2008) Soil Geography and Geostatistics Concepts and Applications. JRC, Institute for Environment and Sustainability, Luxembourg.

[13] Qu, M., Li, W. and Zhang, C. (2013) Assessing the Spatial Uncertainty in Soil Nitrogen Mapping through Stochastic Simulations with Categorical Lande Use Information. *Ecological Informatics*, **16**, 1-9. https://doi.org/10.1016/j.ecoinf.2013.04.001

[14] Deutsch, C.V. and Journel, A.G. (1998) GSLIB: Geostatistical Software Library and User's Guide. Oxford University Press, New York.

[15] Goovaerts, P. (1997) Geostatistics for Natural Resources Evaluation. Oxford University Press, New York.

[16] Felgueiras, C.A. (1999) Modelagem Ambiental Com Tratamento De Incertezas Em Sistemas De Informação Geográfica: O Paradigma Geoestatístico Por Indicação. 165p. Tese (Doutorado em Computação Aplicada), Instituto Nacional de Pesquisas Espaciais, São José dos Campos. http://urlib.net/sid.inpe.br/deise/2001/08.03.12.35

[17] Viscarra-Rossel, A.R., Goovaerts, P. and McBratney, A.B. (2001) Assessment of the Production and Economic Risks of Site-Specific Liming Using Geostatistical Uncertainty Modeling. *Environmetrics*, **12**, 699-711. https://doi.org/10.1002/env.471

[18] Searcy, S.W. (1997) Precision Farming: A new Approach to Crop Management. *Texas Agricultural Extension Service*. The Texas A&M University System, College station, Texas, 4. http://lubbock.tamu.edu/files/2011/10/precisionfarm_1.pdf

[19] Ortiz, J.O (2008) Análise De Risco Na Fase De Palnejamento Em Sistemas De Produção Agrícola Por Meio De Simulação Geosestatística Condicionada. Tese de

Doutorado, INPE, São José dos Campos, SP, Brazil.
http://urlib.net/8JMKD3MGP8W/33JR7HB

[20] Raij, B.V. (1991) Fertilidade Do Solo E Adubação. Ceres, São Paulo, 343 p.

[21] Quaggio, J.A. (2004) Manejo Da Acidez Do Solo E A Prática Da Calagem: Acidez E Calagem Em Solos Tropicais. Instituto Agronômico, Campinas-SP, Artigo técnico da Calpar-calcário agrícola, Paraná.
http://www.calpar.com.br/calpar.com.br/calpar-site2015/artigos-boletim2.html

[22] Buttafuoco, G., Conforti, M., Robustelli, G. and Scariciglia, F. (2011) Assessing Spatial Uncertainty in Mapping Soil Erodibility Factor Using Geostatistical Stochastical Simulation. *Environmental Earth Science*, **66**, 1111-1125.
https://doi.org/10.1007/s12665-011-1317-0

[23] Heuvelink, G.B.M. (1998) Error Propagation in Environmental Modeling with GIS. Taylor and Francis Inc., Bristol, 127 p.

[24] Suro Perez, V.S. and Journel, A.G. (1991) Indicator Principal Component Kriging. *Mathematical Geology*, **23**, 759-793. https://doi.org/10.1007/BF02082535

[25] Richards, J.A. (1996) Remote Sensing Digital Image Analysis: An Introduction, Chapter 6. Springer Verlag, Berlin, 280 p.

[26] Journel, A.G. (1983) Nonparametric Estimation of Spatial Distributions. *Mathematical Geology*, **15**, 445-468. https://doi.org/10.1007/BF01031292

[27] Goovaerts, P. (2001) Geostatistical Modelling of Uncertainty in Soil Science. *Geoderma*, **103**, 3-26. https://doi.org/10.1016/S0016-7061(01)00067-2

[28] Impar-Consultoria e Assessoria Agrícola (2005). http://www.imparag.com.br/

[29] Camara, G., Souza, R.C.M., Freitas, U.M and Garrido, J.G. (1996) SPRING: Integrating Remote Sensing and GIS by Object-Oriented Data Modelling. *Computers & Graphics*, **20**, 395-403. https://doi.org/10.1016/0097-8493(96)00008-8

Scientific Research Publishing

Open Journal of Soil Science, 2017, 7, 149-171
http://www.scirp.org/journal/ojss
ISSN Online: 2162-5379
ISSN Print: 2162-5360

Relating Cone Penetration and Rutting Resistance to Variations in Forest Soil Properties and Daily Moisture Fluctuations

Marie-France Jones, Paul A. Arp

Forest Watershed Research Centre, Faculty of Forestry and Environmental Management, University of New Brunswick, Fredericton, Canada
Email: arp2@unb.ca

How to cite this paper: Jones, M.-F. and Arp, P.A. (2017) Relating Cone Penetration and Rutting Resistance to Variations in Forest Soil Properties and Daily Moisture Fluctuations. *Open Journal of Soil Science*, **7**, 149-171.
https://doi.org/10.4236/ojss.2017.77012

Received: May 19, 2017
Accepted: July 14, 2017
Published: July 17, 2017

Abstract

Soil resistance to penetration and rutting depends on variations in soil texture, density and weather-affected changes in moisture content. It is therefore difficult to know when and where off-road traffic could lead to rutting-induced soil disturbances. To establish some of the empirical means needed to enable the "when" and "where" determinations, an effort was made to model the soil resistance to penetration over time for three contrasting forest locations in Fredericton, New Brunswick: a loam and a clay loam on ablation/ basal till, and a sandy loam on alluvium. Measurements were taken manually with a soil moisture probe and a cone penetrometer from spring to fall at weekly intervals. Soil moisture was measured at 7.5 cm soil depth, and modelled at 15, 30, 45 and 60 cm depth using the Forest Hydrology Model (ForHyM). Cone penetration in the form of the cone index (*CI*) was determined at the same depths. These determinations were not only correlated with measured soil moisture but were also affected by soil density (or pore space), texture, and coarse fragment and organic matter content (R^2 = 0.54; all locations and soil depths). The resulting regression-derived *CI* model was used to emulate how *CI* would generally change at each of the three locations based on daily weather records for rain, snow, and air temperature. This was done through location-initialized and calibrated hydrological and geospatial modelling. For practical interpretation purposes, the resulting *CI* projections were transformed into rut-depth estimates regarding multi-pass off-road all-terrain vehicle traffic.

Keywords

Soil Resistance to Penetration, Cone Index, Soil Moisture, Texture, Coarse Fragments, Organic Matter, Weather Records, Hydrological Modelling, Soil Trafficability, Rutting Depth, Recreational Vehicles

1. Introduction

The soil cone index (*CI*), a measure of a soil's resistance to penetration (*MPa*), is a commonly used soil mechanical property to determine soil strength [1] [2]. This strength generally increases with increasing clay, coarse fragment (*CF*), and soil density (D_b), or reduced pore space (*PS*), but decreases with increasing soil moisture (*MC*) and organic matter content (*OM*, %) [3] [4] [5] [6]. Hence, non-cohesive soils such as sands and sandy loams are more easily penetrated than clay soils [3] [7] [8], wet soils have low penetration resistances and the resistance to penetration is low for organically enriched soils but high for stony and frozen soils [9] [10] [11].

In practice, off-road traffic may increase soil compaction and *CI*, which negatively affects the growth of crops by way of reduced root development [8] [12] [13] [14] [15]. In urban developments, increased *CI* due to soil compaction decreases soil infiltration of water and tree root growth [16] [17]. However, sufficient *CI*-index soil strength is needed to allow on- and off-road traffic in agriculture and forestry operations [18] [19], while off-road recreational traffic needs to be controlled to avoid soil rutting. In this, the resistance of soils to rutting is directly proportional to the ratio between tire footprint pressure and *CI* [20] [21] [22]. The former increases with increasing vehicle weight and load and decreasing tire footprint, which—in turn—decreases with increasing tire width, wheel diameter, and decreasing tire pressure. In the field, rut depths further increase from single to multiple passes, and with slope-induced tire spinning [23].

Efforts to minimize soil rutting require reliable forecasting of off-road soil trafficability. Doing this, however, is challenging because soil and machine-use conditions may vary daily from location to location. By location, low *CI* conditions do not last as long for sandy soils than for loams and clays. In addition, soil trafficability varies with the extent of soil freezing and thawing, especially when traffic turns thawing soils into mud [24].

The objective of this article is determining how manually derived soil *CI* determinations change in response to weekly spring-to-winter changes in soil moisture and temperature for three contrasting soil conditions. The data so generated allowed for: 1) quantifying the relationship between *CI* and soil *MC*; 2) emulating and interpreting the changes in soil moisture, *CI*, and rutting depth; 3) daily year-round modelling of soil trafficability by soil texture and soil depth. While machine-based cone penetration testing (*CPT* [25]) would be more accurate and precise, manual *CI* determinations have the greater portability and affordability advantage for assessing how soil trafficability conditions vary from location to location across landscapes and seasons.

2. Materials and Methods

2.1. Location Description

Three forest sites in Fredericton, New Brunswick, were chosen for this study

(Figure 1, Table 1):

1) A mixed-wood stand on sandy clay loam in a wooded section on the University of New Brunswick campus (*UNB*);

2) A hemlock (*Tsuga canadensis*) stand on a rich loam in Odell Park (*OP*);

3) A silver maple site (*Acer saccharinum*) on an alluvial sandy loam next to a fresh-water marsh within the floodplain of the Nashwaaksis stream (*SM*).

The two non-alluvial soils developed on grey sandstone ablation / basal till. Elevation for the three sites ranges from 6 to 70 m [26]. The topography varies from undulating to hilly. The upland forest vegetation is representative of the Acadian forest species, *i.e.*, sugar maple (*Acer saccharum*), red maple (*Acre rubrum*), white birch (*Betula papyrifera*), balsam fir (*Abies balsamea*), black spruce (*Picea mariana*), and hemlock (*Tsuga canadensis*). The 1950-2017 Fredericton weather record has a mean annual temperature of 6.6˚C, with monthly means of −1.8 and 14.9˚C for January and July, respectively. Mean annual precipitation amounts to 1100 mm, including 250 mm of snow [27].

2.2. Field Experiment

Soil layers were described and samples were taken from two freshly dug soil pits at each of the three locations. Five soil volumetric moisture content (MC_v) and *CI* readings were taken manually each week from May 29, 2015 to November 2, 2015 within two circular plots (1.5 m radius) near the soil pits at each location. This was done using a Delta T HH2 moisture meter and a Humboldt digital cone penetrometer (cone are at base = 1.5 cm^2; cone angle 60˚). The MC_v readings were taken at 7.5-cm mineral soil depth. The *CI* readings were obtained at 15, 30, 45, and 60 cm depths, but were not recorded where obstructed by logs, coarse roots, and surface-accumulated rocks.

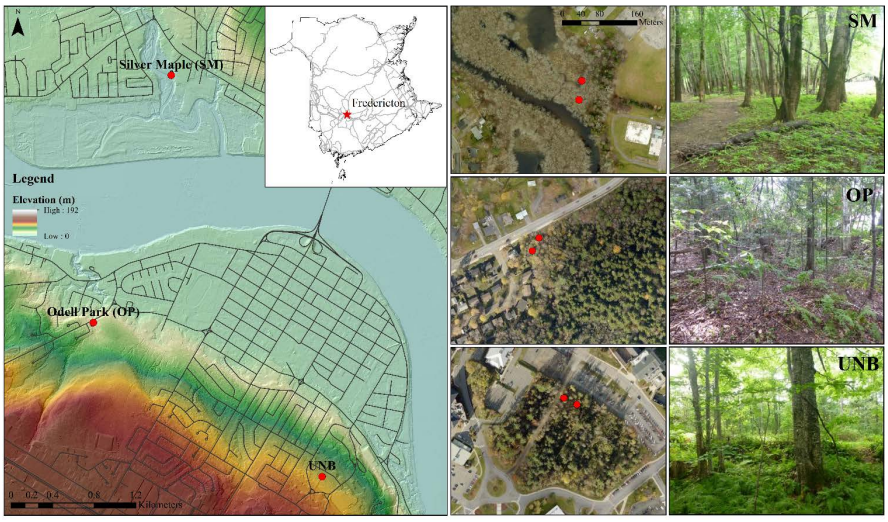

Figure 1. Overview depicting of the three Fredericton (New Brunswick) locations (left), and site-specific plot locations for *SM* (top), *OP* (middle), *UNB* (bottom) (Imagery Source: Esri, DigitalGlobe, GeoEye, Earthstar Geographics, CNES/Airbus DS, USDA, USGS, AEX, Getmapping, Aerogrid, IGN, IGP, swisstopo, and the GIS User Community).

Table 1. Location descriptions used for initializing ForHyM.

Location Parameters	UNB	SM	OP
Latitude (N)	45˚56'40"	45˚57'28"	45˚58'46"
Longitude (W)	66˚38'34"	66˚40'17"	66˚39'44"
Elevation (m)	70	8	29
Slope (%)	4.45	2.46	2.71
Aspect (°)	30	132	24
Canopy Coverage Deciduous: Coniferous	20:40	70:0	30:30
Rooting habit	Shallow	Deep	Shallow
Forest floor thickness (cm)	8	2	5
Soil Series	Sunbury / Till	Riverbank / Glaciofluvial Deposits	Sunbury / Till
Soil Classification	Gleyed Sombric Brunisol	Gleyed Humic Regosol	Orthic Humo-Ferric Podzol
Mineral soil texture	Sandy loam	Loamy sand– Sandy loam	Silty loam– Sandy loam
Subsoil texture	Sandy loam	Loamy sand	Silty loam

The soil samples were placed into labeled freezer bags for storage. Prior to analysis, the samples were dried in a forced-air oven 75˚C for 24 hours, crushed with a mortar and pestle, and passed through a 2-mm sieve to remove and to determine the *CF*. The fine-earth fraction was used to determine its sand, silt, and clay content using the hydrometer method [28]. The soil carbon content (C) of this fraction was determined using a LECO CNS-2000 analyzer. Soil OM content was estimated by weight by setting $OM_g\% = 1.72 \times C\%$. The pore-space filled moisture content (MC_{ps}) was inferred by assuming that soil gravimetric moisture content (MC_g), soil bulk density (D_b) and the PS percentage would be affected by depth and OM content as follows [3]:

$$D_b = \frac{1.23 + \left(D_p - 1.23\right) \times \left[1 - \exp\left(-0.0106 \times DEPTH\right)\right]}{1 + 6.83 \times OM_W} \quad (1)$$

$$MC_g = MC_v \times D_b \quad (2)$$

$$MC_{ps} = \frac{MC_v}{PS} \quad (3)$$

where D_p is particle density (2.65 g/cm^3), and PS is the pore space fraction of the fine earth.

2.3. Hydrological Modelling

The forest hydrology model (ForHyM) [29] [30] [31] was used to emulate the changes in daily soil moisture, soil temperature and snowpack conditions for

each of the three locations from 2006 to 2017. Doing this involved compiling the daily Fredericton weather records for air temperature, precipitation (rain, snow), stream discharge, and open-ground snow depth [27] [32]. Also specified were elevation, slope, aspect, and extent of forest cover (**Table 1**). The model-internal water and heat flow parameters pertaining to soil permeability, thermal conductivity, and heat capacity were plot-adjusted by texture, *OM* and *CF* content (**Table 2**), and by comparing actual with modeled soil moisture content. This was done through manually resetting the default values for: 1) the air-to-snowpack heat-transfer coefficient; 2) the initial snowpack density of freshly fallen snow to reflect the open-ground conditions at the weather station [33]; and 3) the lateral soil permeability to account for lateral flow tortuosity [34] [35]. These adjustments ensured that the model output conformed to actual snowpack depth and stream discharge records.

2.4. Data Analysis and Model Projections (MC_v, *CI*, Rut Depth)

The data and ForHyM estimates for MC_v, *CI*, texture, *CF*, *OM*, D_b, and *PS* were entered into a spreadsheet by location, date, and soil depth. This compilation served 1) to generate basic statistical summaries, 2) to analyze the measured and modelled time-series plots for MC_v and *CI*, and 3) to determine the best-fitted linear and multiple regression models with *CI* as dependent variable, and with MC_v (measured, modelled), soil texture, *OM*, *CF*, *PS*, and soil depth as independent variables. A linear regression model served to relate measured *CI* at 15, 30, 45 and 60 cm soil depth to measured and ForHyM-modelled MC_v. A multiple regression model served to relate *CI* to MC_v, *PS*, and *CF* as follows:

$$\log_{10} CI = a + bPS + cMC_{ps} + dCF \tag{4}$$

where MC_{ps} is the water-filled portion of the *PS*, in percent. The best-fitted model so generated was incorporated into the ForHyM model to determine how MC_v, *CI* and rutting depths pertaining to all-terrain vehicle (*ATV*) traffic would vary over time at each of the three locations. The equations adopted for rut modelling were as follows [4] [36]:

Potential rut depths for n passes:

$$RD_n = \left(\frac{1656}{NCI}\right) n^{\frac{1}{2}} \tag{5}$$

with *NCI* (the nominal cone index) given by:

$$NCI = -\frac{1000\, CI\, bd}{W}\sqrt{\frac{\delta}{h}}\frac{1}{1+2d} \tag{6}$$

where b is tire width (m), d is tire diameter (m), h is section height (m), δ is tire deflection (m) given by 0.008 + 0.001 (0.365 +170 / p), p is tire inflation pressure (kPa), W is vehicle weight + load (kN) per wheel, and n is number of vehicle passes along the same track. Potential rutting depths for all-terrain recreational vehicle (*ATV*) traffic were determined using the following machine specifications: number of wheels = 4; W per wheel = 3.1 kN; b = 0.254 m; d = 0.62 m; h = 0.3 m; p = 34.4 kPa; n = 10 passes.

Table 2. ForHyM initialization requirements by soil layer per plot and location.

Location	Plot	Layers	Depth (cm)	Sand (%)	Clay (%)	Silt (%)	OM (%)	CF (%)	Rooting
UNB	1	LF	−8 - 0		Organic		100	0	Plentiful fine
		Ah	0 - 15	43	14	43	25	1	Plentiful fine
		Bmg	15 - 40	66	10	24	5	10	Abundant med-fine
		Cxg1	40 - 70	66	10	24	1	20	Few coarse
		Cxg2	70+	66	10	24	0	70	
	2	LF	−8 - 0		Organic		1	0	Plentiful fine
		Ah	0 - 15	43	17	40	7	1	Plentiful fine
		Bmg	15 - 40	66	10	24	2	10	Abundant med-fine
		Cxg1	40 - 70	66	10	24	1	20	Few coarse
		Cxg2	70+	66	10	24	0	50	
SM	1	L	−2 - 0		Organic		100	0	
		Ah	0 - 15	48	17	35	10	0	Abundant fine
		Cg1	15 - 65	44	17	39	5	10	Few coarse
		Cg2	65 - 105	35	18	47	0	15	Few coarse
		Cg3	105+	35	18	47	0	15	
	2	L	−2 - 0		Organic		100	0	
		Ah	0 - 15	48	17	35	20	0	Abundant fine
		Cg1	15 - 45	44	17	39	10	5	Few coarse
		Cg2	45 - 95	35	18	47	0	10	Few coarse
		Cg3	95+	35	18	47	0	15	
OP	1	LFH	−5 - 0		Organic		1	0	Plentiful fine
		Ahe	0 - 15	58	18	24	10	1	Plentiful fine to med
		Bf	15 - 40	54	20	26	5	5	Abundant med
		BC	40 - 90	54	20	26	1	10	Few coarse
		C	90+	56	12	32	0	10	
	2	LFH	−5 - 0		Organic		1	0	Plentiful fine
		Ahe	0 - 15	58	18	24	10	1	Plentiful fine to med
		Bf	15 - 35	54	20	26	5	15	Abundant med
		BC	35 - 70	54	20	26	1	15	Few coarse
		C	70+	56	12	32	0	15	

To visually represent the temporal changes in *MC* topographically and over seasons, MC_{ps} was spatially related to the depth-to-water index (*DTW*). This as index was generated from a 1-m resolution bare-earth digital elevation model (*DEM*) for the Fredericton area [37]. This index determines the elevation rise along the least slope path from each cell across the landscape to its nearest open-water cell corresponding to streams, lakes, rivers and open shores [38] [39].

Changing the upslope flow-accumulation area by channel flow initiation (*FI*), *i.e.*, changing the amount of upstream area needed to initiate streamflow, allows for indexing *DTW* by season. For example, *FI* = 4 ha generally represents permanent stream flow at the end of summer, *FI* = 0.25 ha represents the extent of ephemeral stream flow during and after snowmelt, and *FI* = 1 ha represents channel flow during the transitional periods from fall to winter. The resulting *DTW* rasters with *FI* = 4, 1 and 0.25 ha were used to determine how the soil moisture conditions and rutting depths would vary across the terrain associated for the three sampling locations by season. This was done by applying Equation (7) and Equation (8) [3], *i.e.* [40]:

$$MC_{PS} = 1 - \left[1 - MC_{PS}\left(DTW_{ridge}\right)\right] * \left[\frac{1 - \exp\left(-k * DTW\right)}{1 - \exp\left(-k * DTW_{ridge}\right)}\right]^{p} \quad (7)$$

$$RD_{n} = RD_{n,ridge} - \left[RD_{n,ridge} - RD_{n,DTW=0}\right] * \left[\frac{1 - \exp\exp\left(-k * DTW\right)}{1 - \exp\exp\left(-k * DTW_{ridge}\right)}\right]^{p} \quad (8)$$

with $p = 2$, p as soil-specific parameter ranging from 0.2 to 2 and), and DTW_{ridge} (in m) R$D_{n,ridge}$ and $RD_{n,DTW=0}$ (in mm) determined for driest and wettest parts of each.

3. Results

3.1. Soil Moisture and *CI* Measurements

Each of the three locations showed distinct variations in soil properties, strength, and moisture readings over the course of 23 weeks. Given the plot-by-plot soil property differences—and tracking the changes in soil moisture over time—revealed that the *OP* plots drained quickly. In contrast, the *UNB* plots varied the most from wet to dry and back again to wet from spring to fall (**Figure 2**). In direct correspondence, resistance to cone penetration varied the least for the two *SM* plots, and the most for the *UNB* plots. These differences arose from the compacted and poorly drained sandy loam for the *UNB* plots, the well-drained loamy sand with low *CF* content for the *OP* plots, and seasonally recurring flooding of the *SM* plots (**Table 1** and **Table 2**). The high springtime levels for MC_v within the top 15-cm soil at the *UNB* and *SM* locations are due to high Ah-layer *OM* content, which—according to Equation (1)—lowers D_b and enhances the soil-filled *PS* between the coarse fragments.

Plotting the *CI* measurements at 15 cm depth to the MC_v measurements revealed that the log-transformed *CI* and MC_v values are linearly related to one another as shown in **Figure 3** (left), as follows:

$$\log_{10} CI_{15cm} = 0.62\left(\pm 0.07\right) - 0.52\left(\pm 0.05\right)\log_{10} MC_{v} + 0.20\left(\pm 0.03\right)UNB \quad (9)$$

R^2 = 0.60, *RSME* = 0.13, *MAE* = 0.10, with the *UNB* location coded 1 and 0 otherwise. Similarly similar strong correlations between *MC* and *CI* have been reported elsewhere [5] [41] [42]. With respect to increasing soil depth—and as

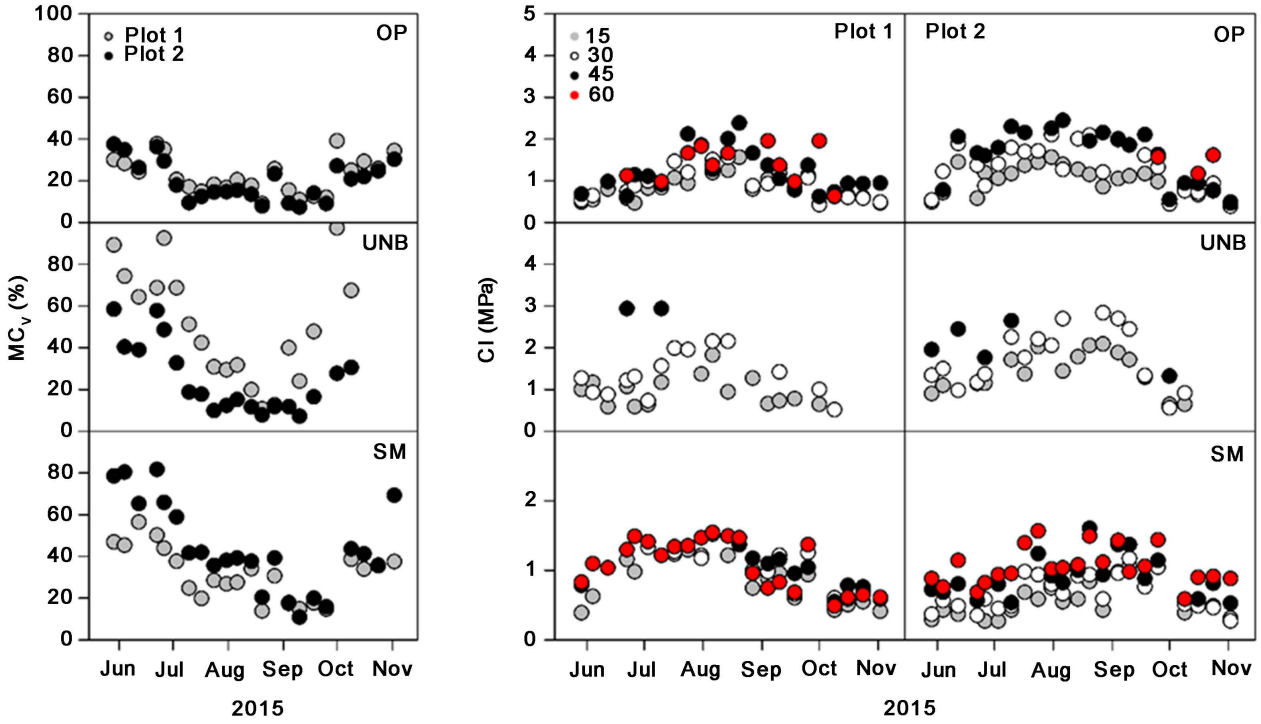

Figure 2. Left: Measured MC_v for the top 15 cm of soil. Right: Measured *CI* at 15, 30, 45, and 60 cm depth for Plots 1 and 2 at the *OP*, *UNB*, and *SM* locations.

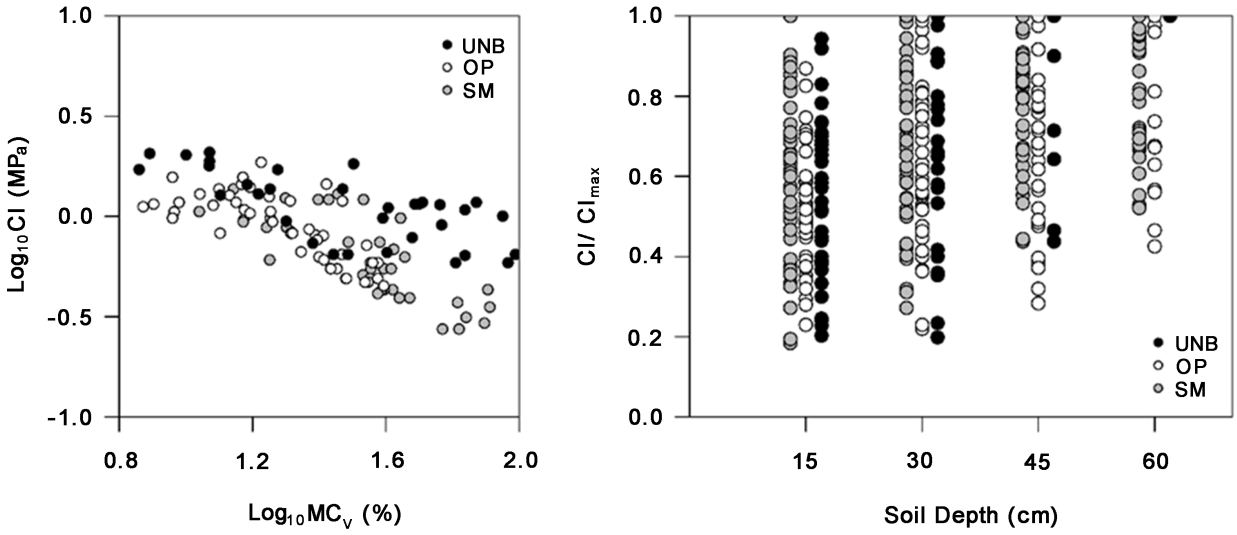

Figure 3. Scatterplots of measured $\log_{10}CI$ versus measured $\log_{10}MC_v$ (left), and weekly of CI / CI_{max} averages for the *OP*, *UNB*, and *SM* locations (right).

shown in Figure 3 (right)—*CI* increases, by plotting the ratio of the weekly averages of *CI* over CI_{max} per plot by location. A similar trend has also been reported elsewhere [43] [44] [45].

3.2. Soil Moisture and *CI* through Hydrological Modelling

The modelling of the year-round soil moisture conditions required plot-specific

ForHyM initializations and calibrations. These included the Fredericton-specific calibrations for snowpack depth and stream discharge required using daily Fredericton Airport weather records for rain, snow and air temperature, and adjusting the ForHyM-default settings for lateral and downward water flow, as listed in Table 3. The plot initializations in Table 1 and Table 2 refer to entering the plot- and/or layer-specific values for slope, aspect, vegetation type and cover, forest floor depth, percentages for sand, silt, clay, *CF*, *OM*, and layer depth.

Shown in Figure 4 are the resulting time-series plots for daily air temperature and precipitation (input), snowpack depth, stream discharge, top 15-cm soil MC_v (actual and modelled), and frost depth (modelled). The resulting scatter plots in Figure 5 for actual and best-fitted ForHyM snowpack depth and top 15-cm MC_v (top 15 cm) demonstrate a reasonable good fit, with $R^2 = 0.81$ for snowpack depth, 0.62 for stream discharge, and 0.76 for MC_v (Table 4).

For the purpose of predicting how *CI* would vary across time by soil texture, D_b and *CF* content (Table 2), it was necessary to use the ForHyM-generated depth- and time-dependent MC_v output for the 0 - 15, 15 - 30, 30 - 45 and 45 - 60 cm soil layers as predictor variable. Doing this involved estimating how much of the infiltrating and percolating water would be retained at any time within the fine-earth fraction between the coarse fragments of each layer. For example, the space available for water retention would decrease with increasing *CF* content. Consequently, there would be less *PS* to fill between the coarse fragments during wet weather conditions, and there would also be less water available for root uptake during warm summer weather [46]. This being so, The ForHyM-generated projections in Figure 6 by location and soil layer show greater MC_v and MC_{ps} variations for the stony *UNB* location, followed by the less stony *SM* and the more sandy *OP* locations. In combination, the ForHyM projections in Figure 6 capture the plot-by-plot MC_{ps} variations such that $OP_{MC} > SM_{MC} > UNB_{MC}$.

Figure 7 and the correlation coefficients in Table 5 show how *CI* varies with varying soil texture (Sand), *CF*, *OM*, *PS* and MC_{ps}. In general, *CI* decreases with

Table 3. ForHyM calibrations for the Fredericton area: default multipliers.

Parameters		Multiplier
Snowpack	Snow-to-air temperature gradient	0.16
	Density of fresh snow	0.20
Saturated soil permeability	Surface runoff	1
	Forest floor infiltration	1
	Forest floor interflow	0.05
	A&B horizon infiltration	1
	A&B horizon interflow	0.1
	C horizon infiltration	1
	C horizon interflow	0.1
	Deep water percolation	1

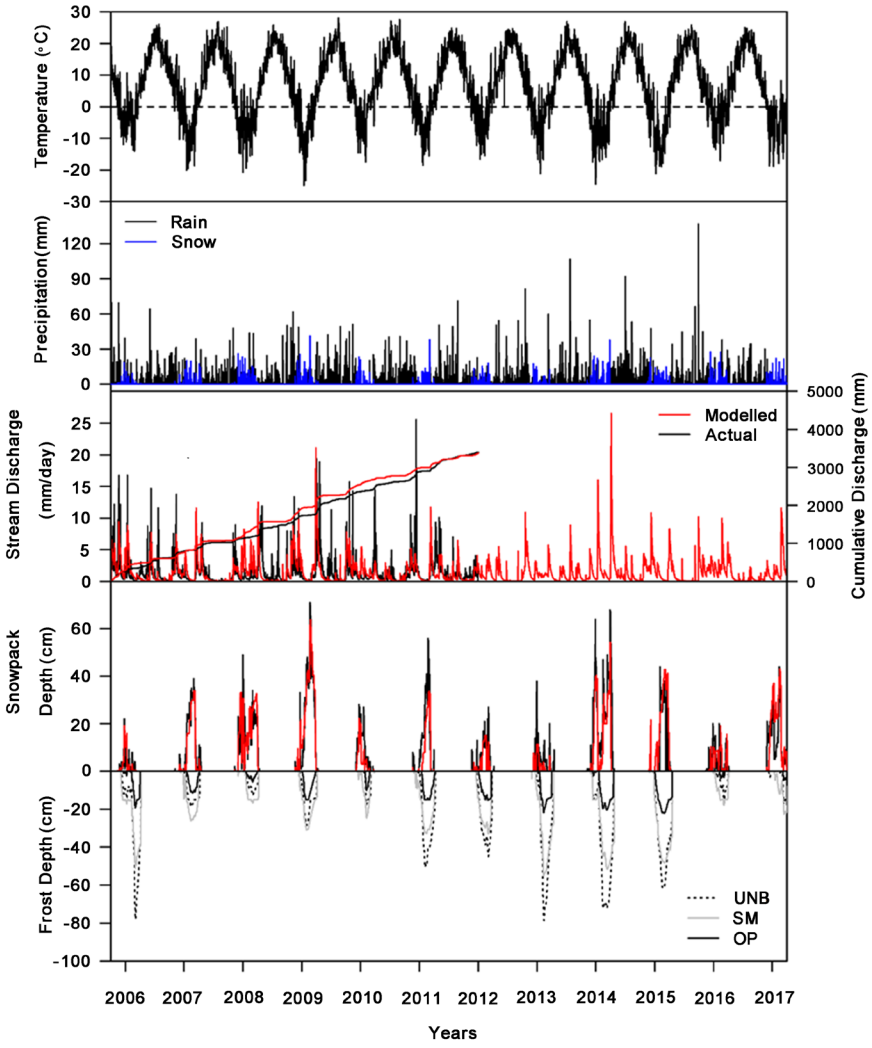

Figure 4. ForHyM time-series plots for daily air temperature and precipitation (ForHyM input), actual and modelled output for stream discharge and snowpack depth, and location-specific modelled frost depth (modelled).

increasing *PS* and sand content due decreasing particle-to-particle contacts. Increased *OM* content decreases *CI* by way of soil aggregation, i.e. by further loosening the point of contact among the aggregated soil particles. The *CF*-induced increase on *CI* refers to the increasing strength needed to displace the coarser particles away from cone penetration path [47]. Together, Sand, *OM*, *CF* and *PS* affect the daily variations in *CI* and soil moisture retention through their combined effect on soil pore space, texture, structure and drainage [33] [48] [49].

Subjecting the correlation matrix in **Table 6** to factor analysis revealed that the *CI* variations can be grouped into three *CI*-determining factors. Factor 1 is the Location Factor, which relates a component of the *CI* variations to the location- and layer-specific *CF* and *PS* determinations. Factor 2 is the Soil Moisture Factor, which relates some of the *CI* variations to MC_{ps}. Factor 3 is strongly related to Sand, but—in this formulation—has no salient effect on *CI*.

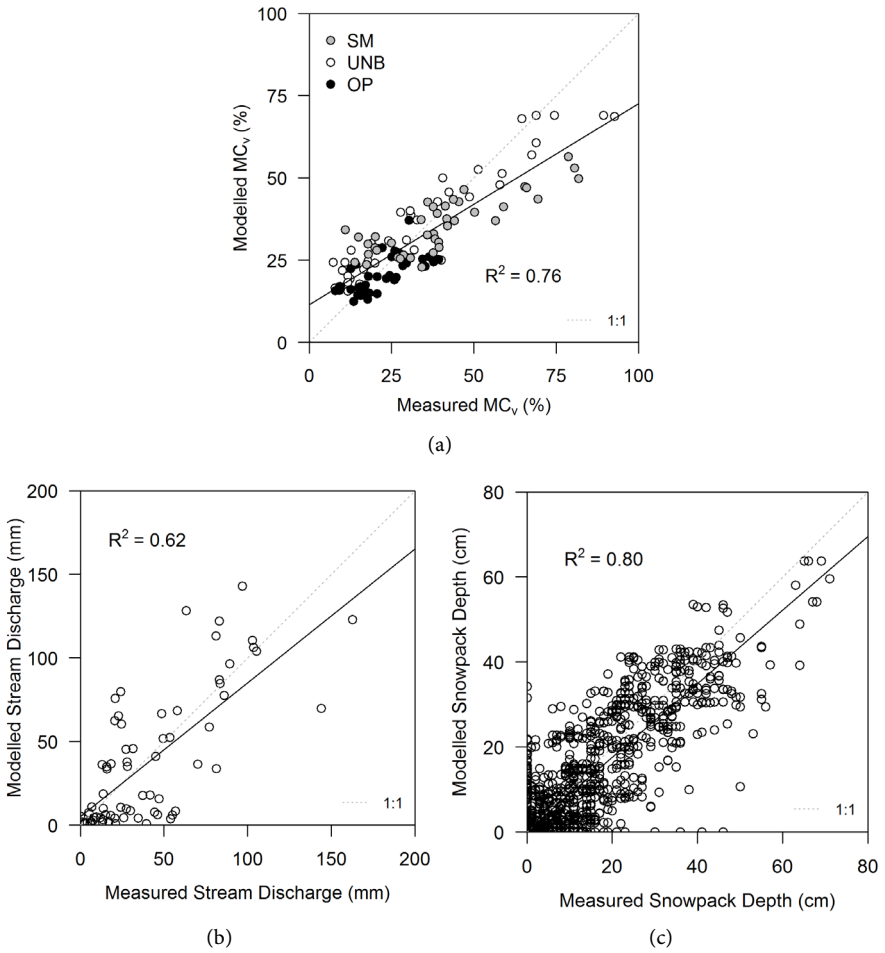

Figure 5. Actual versus ForHyM best-fitted scatter plots for MC_v (top 15 cm) (left), monthly stream discharge (middle), and daily snowpack depth (right).

Table 4. Best-fitted regression model for measured (actual) versus modelled top 15-cm soil MC_v by location (*UNB*, *SM*, *OP*) and overall.

Parameter	n	Intercept		Coefficient		*t-value*	*p-value*	*Adj. R²*	*RMSE*	*MAE*
		Estimate	SE	Estimate	SE					
UNB	37	13.884	1.690	0.676	0.039	17.308	<0.001	0.90	5.47	4.50
SM	41	20.541	1.816	0.384	0.041	9.173	<0.001	0.67	4.77	3.91
OP	41	11.694	1.748	0.415	0.073	5.717	<0.001	0.44	4.01	3.06
All Sites	118	11.527	1.191	0.611	0.032	19.365	<0.001	0.76	6.57	5.48

Using *PS*, MC_{ps}, and *CF* as independent variables produced the following best-fitted multiple regression result for all soil layers and locations combined:

$$\log_{10} CI = 0.26 - 0.29PS - 0.41MC_{PS} + 1.04CF \quad (10)$$

$R^2 = 0.54$, $RMSE = 0.36$, $MAE = 0.29$. This result is illustrated in Figure 8 by way of the 3D plots, which reveal moderate *CI* increase with decreasing MC_{ps}, and a rapid *CI* increase with increasing *CF*. In reality, *CI* and soil strength should decrease again as MC_{ps} drop towards zero as the soil becomes more brittle due to reduced particle-to-particle hydrogen-bonding at low *MC* [50].

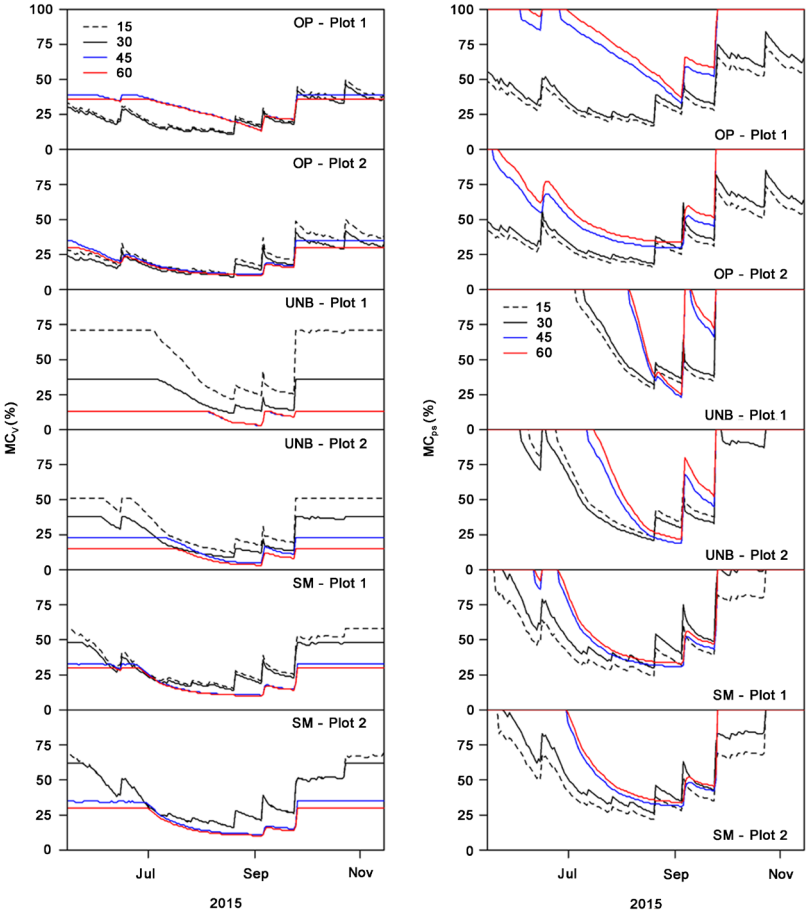

Figure 6. ForHyM-generated MC_v and MC_{ps} projection for the 0 - 15, 25 - 30, 30 - 45 and 45 - 60 cm soil layers by plot and location.

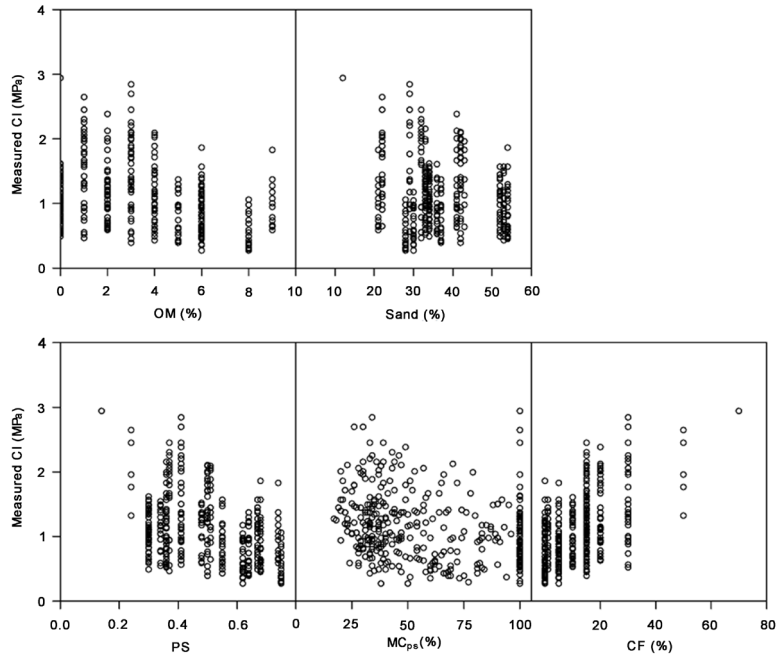

Figure 7. Plotting plot-by-plot measured *CI* vs. *OM*, Sand, *PS*, MC_{ps}, and *CF*, showing *PS*, MC_{ps}, and *CF* as stronger *CI* predictor variables than *OM* and Sand.

Table 5. Correlation matrix for plot- and layer-determined *CI*, *OM*, Sand, *CF* and ForHyM-estimated D_b, MC_v, MC_{ps}.

Variables	CI	MC_{ps}	MC_v	SP	CF	Sand	Db	OM
CI	1.00							
MC_{ps}	−0.26	1.00						
MC_v	−0.52	0.72	1.00					
SP	−0.39	−0.37	0.32	1.00				
CF	0.55	0.35	−0.18	−0.74	1.00			
Sand	−0.16	−0.30	−0.20	0.21	−0.42	1.00		
Db	0.39	0.37	−0.32	−1.00	0.73	−0.20	1.00	
OM	−0.31	−0.31	0.36	0.97	−0.59	0.07	−0.97	1.00

Table 6. Factor analysis of **Table 5**.

Parameters	Factor 1	Factor 2	Factor 3
CI	0.72	0.75	−0.02
MC_{ps}	0.18	−0.88	−0.26
SP	−0.92	0.11	−0.09
CF	0.86	0.03	−0.23
Sand	0.00	0.15	1.00

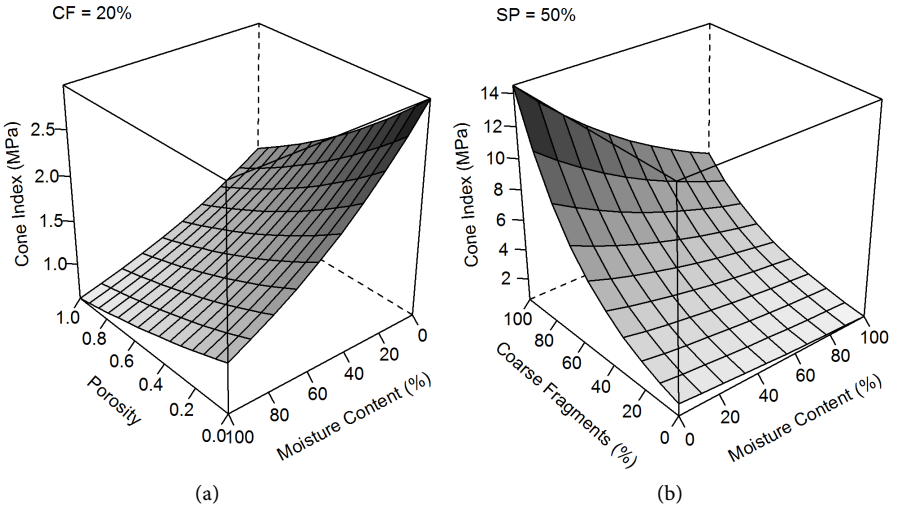

Figure 8. Modelled *CI* (Equation (10)) in relation (a) to MC_{ps} and *PS* at *CF* = 20%; and (b) to *CF* and MC_{ps} at *SP* = 20%.

While Sand and *OM* are important water retention and porosity predictor variables [51] [52], including them as part of the multiple regression process did not significantly improve the best-fitted results, likely due to the significant correlations between *OM* and *PS* and between Sand and *CF* in **Table 5**. However, adding sampling location to the predictor variables (each location coded 1 where applicable, else 0) improved the best-fitted result as follows:

$$\log_{10} CI = 0.44 - 0.50PS - 0.39MC_{PS} + 0.69CF - 0.09SM \quad (11)$$

R^2 = 0.60, *RMSE* = 0.33, *MAE* = 0.27. This means that the *CI* values at the *SM*

plots are, on average, slightly lower than at the other locations. This difference may be related to unaccounted differences pertaining to, e.g., *CF* size (generally smaller at *SM* than at the other two locations), and differences in rooting pattern.

Repeating this analysis by location and by soil depth produced the best-fitted results listed in Table 7. From this, it can be noted that R^2 remained about the same by location, varying from 0.41 (*SM*) to 0.66 (*UNB*), but decreased with increasing soil depth from 0.68 at the top to 0.10 at 60 cm soil depth. This decrease would mostly be due to the location-by-location D_b, *MC* and *CF* differences. This is because 1) the ForHyM-generated *MC* estimates already take the effect of *CF* on MC_{ps} into account, and 2) the *CI* readings become increasingly erratic when pushed through soils with increasing *CF* content.

The dependency of *CI* data on soil *PS*, *MC* and *CF* content was further evaluated through multiple regression analysis based on literature-generated *CI* formulations (Table 8). The result of so doing indicated that: 1) Equation (10) provides the best data representation overall, 2) the linear formulations for *CI* are somewhat weaker than the logarithmic formulations. Also, 3) soil porosity (or density) and *MC* are the more persistent and significant *CI* predictor variables than either Sand or *CF* alone.

3.3. Predicting Potential ATV-Caused Soil Rutting Depth

ForHyM was used to transform the MC_{ps} and *CI* projections over time into likely ATV-generated rut depths over time from April 2013 to April 2017, using the average top 15-cm *PS* and *CF* values and Equation (7), Equation (8), and Equation (10) the two plots at the three sampling locations. The results are represented by the time-series plot in Figure 9. As to be expected, deepest ruts would be incurred during spring and fall, with minor blips during summer. Ruts could also be incurred during winter when some of the frozen soils would thaw due to interim warm weather and upward geothermal heat flow underneath the heat–insulating snow accumulations [53]. While trafficability advisories exist from fall to spring due to wet soil conditions, such advisories apply regionally, and therefore fall short in terms of local "when" and "where" decisions.

Table 7. Linear regression results for measured vs. modelled *CI* by depth and location.

	n	Intercept		Coefficient		t-value	p-value	Adj. R^2	RMSE	MAE
		Estimate	SE	Estimate	SE					
All depths	380	0.010	0.051	1.040	0.044	23.13	<0.001	0.58	0.34	0.27
15 cm	119	0.039	0.083	1.047	0.092	11.358	<0.001	0.52	0.29	0.24
30 cm	114	−0.057	0.093	1.047	0.075	13.921	<0.001	0.63	0.34	0.28
45 cm	90	−0.206	0.124	1.254	0.098	12.751	<0.001	0.64	0.35	0.28
60 cm	58	0.528	0.187	0.5610	0.163	3.451	0.001	0.16	0.32	0.27
SM	167	0.232	0.068	0.772	0.072	10.722	<0.001	0.41	0.27	0.23
OP	145	−0.472	0.133	1.506	0.118	12.758	<0.001	0.53	0.35	0.27
UNB	69	0.010	0.135	1.022	0.088	11.588	<0.001	0.66	0.38	0.31

Table 8. Review of functional relationship between *CI* and soil properties.

Study	Equation	Coefficient Parameters						Adj. R^2	RMSE	MAE
		a	b	c	d	e	f			
1	$\log_{10} CI = a + bPS + cMC_{ps} + cCF$	0.26 (±0.05)	−0.29 (±0.07)	−0.40 (±0.03)	1.04 (±0.10)			0.52	0.36	0.29
2	$\log_{10} CI = a + bPS + cMC_{ps} + dS$	0.74 (±0.05)	−0.78 (±0.06)	−0.40 (±0.03)	−0.31 (±0.09)			0.36	0.42	0.34
3	$\log_{10} CI = a + bPS + cMC_{ps}$	0.62 (±0.04)	−0.80 (±0.06)	−0.37 (±0.03)				0.33	0.43	0.34
4	$CI = a + bMC + cS + dD_b$	2.26 (±0.13)	−2.21 (±0.17)	−1.50 (±0.24)	−0.001 (±0.01)			0.33	0.42	0.34
5	$\log_{10} CI = a + bMC_v + cD_b$	0.04 (±0.04)	−0.73 (±0.07)	0.12 (±0.02)				0.35	0.21	0.16
6	$CI = a + bM + C + cD_b + dMC_g^2 + eD_g^2 + fMC_gD_b$	0.92 (±0.43)	−3.44 (±1.62)	1.20 (±0.46)	3.89 (±1.47)	−0.26 (±0.14)	−0.85 (±0.64)	0.39	0.42	0.33

1: This study; 2: [4]; 3: [45]; 4: [8]; 5: [54]; 6: [55].

The extent to which soil rutting would be seasonally affected across the general neighbourhood of each of the three location was ascertained through digitally generating the elevation-derived cartographic depth-to-water index (*DTW*) associated with the 4, 1 and 0.25 ha upslope areas for streamflow initiation [40] (**Figure 10**). Using these patterns in combination with Equations (7) and Equations (8) produced the spatial MC_{ps} and potential ATV-related rut-depth maps in **Figure 11**, intended to be representative of the off-road soil trafficability conditions during spring, end of summer and the fall to winter transition. As shown, the *UNB* location has the potential to be the most trafficable among the three locations in summer, but would be worst during spring and fall. In contrast, the *OP* location would have the least traffic impact across the area and seasons based on texture-facilitated soil drainage. However, moderate soil rutting could occur within the 4-ha *DTW* < 1 m zone at *OP*. Overall, the soil rutting conditions follow these sequences: dry weather: *UNB* < *OP* < *SM*; wet weather: *OP* < *SM* < *UNB* (**Figure 9**).

4. Discussion

This article describes ways and means by which the resistance of soils to cone penetration can be analyzed and modeled at the daily level year-round, over many years, and for the varying soil conditions by select locations. The results so obtained are—apart from study-specific biases—generally consistent with what has been reported in the literature. These biases would *inter alia* refer to differences in *CI* methodology by, e.g., cone dimensions, speed of cone penetration, and field versus laboratory testing [4].

While the plot-by-plot determinations of this study are limited to three contrasting forest locations, they are at least representative of how soil moisture, *CI*, and rutting depth vary by soil properties, season and topographic position, as demonstrated through daily and spatial modelling. The extent to which this

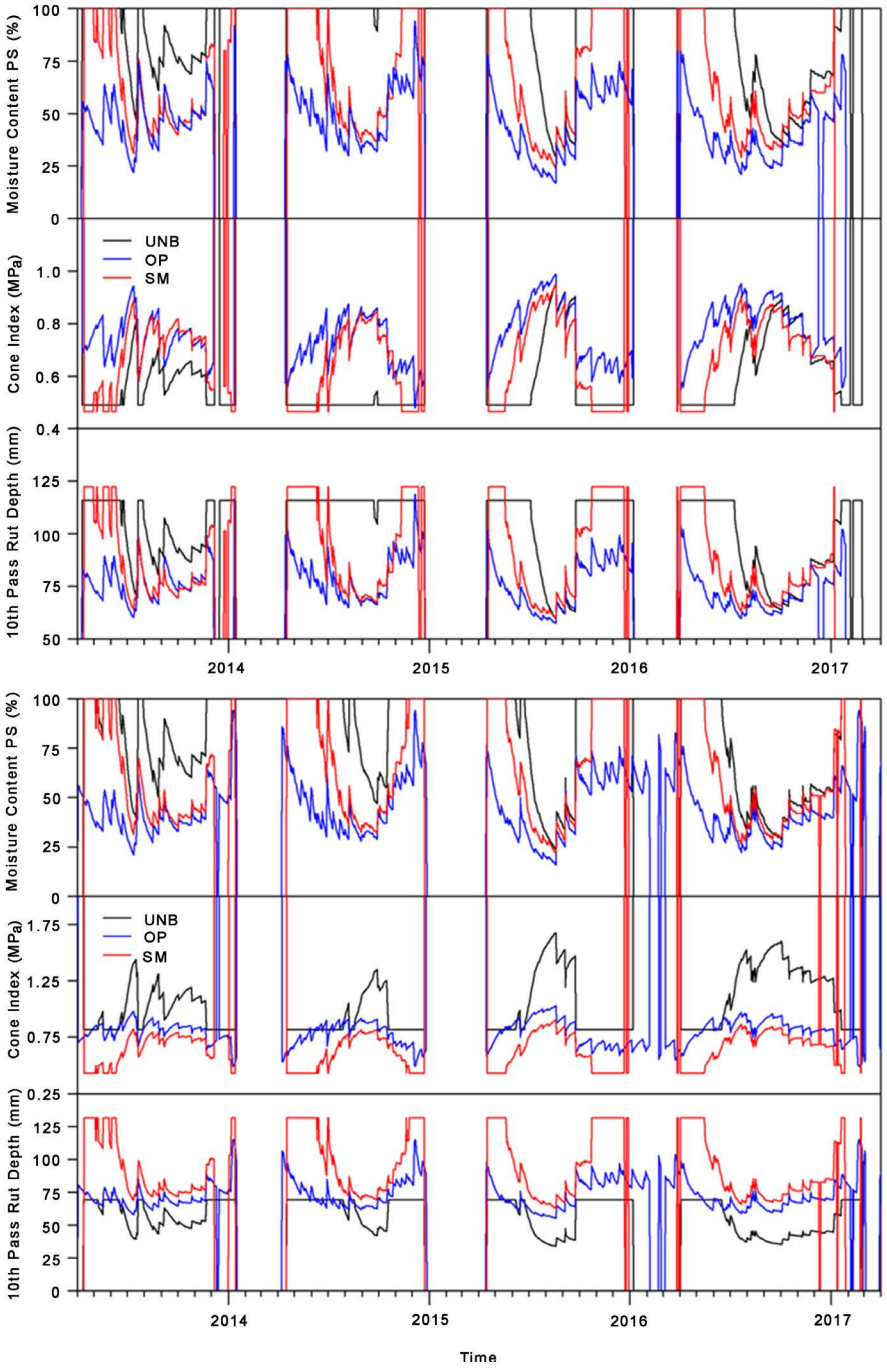

Figure 9. ForHyM-generated unfrozen MC_{ps}, *CI*, and rut depths from April 2013 to April 2017 for the topsoil (top 15 cm of soil) for plot 1 (top) and plot 2 (bottom) at *UNB*, *OP*, and *SM*.

approach can be generalized requires additional research. For example, the spatial and *DTW*-dependent soil trafficability formulation for *CI* and rut depth should be tested across a wider range of glaciated and non-glaciated landforms. Doing so would involve extending the above regression analyses across a wider range of independently varying soil types and properties. For example, where soils are cemented because of pedogenic Fe and Ca accumulations, the approach

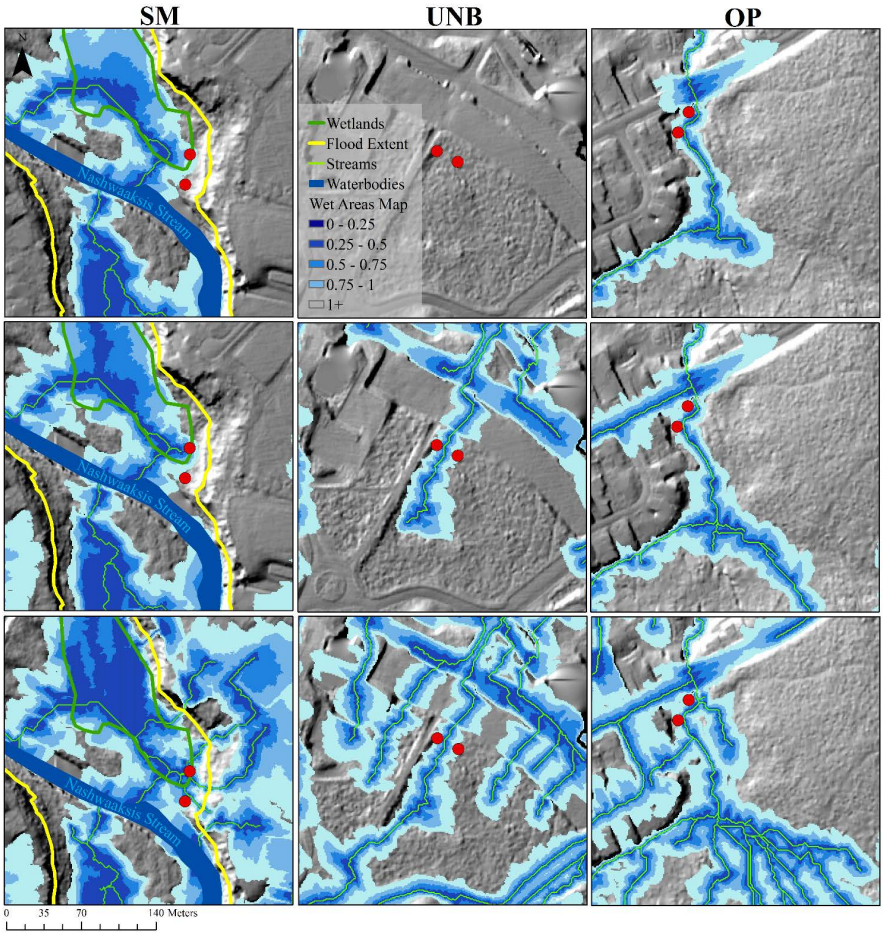

Figure 10. Cartographic depth-to-water index ($DTW \leq 1$ m), overlain on the hill-shaded LiDAR-derived bare-earth digital elevation model for the *UNB*, *OP*, and *SM* locations for end-of-summer (top), spring-to-summer as well as fall-to-winter (middle), and early-spring, as emulated using upslope stream-flow initiation areas amounting to 4, 1 and 0.25 ha, respectively.

would need a cementation predictor variable. In some cases, the mix of the best-fitting regression variable and regression coefficients may also differ, as demonstrated above in Table 8.

Key to applying the approach across time and landscapes is the ability to estimate how soil trafficability changes in direct response to the spatially and temporally varying topo-pedo-hydrological conditions, meter-by-meter. Traditional soil survey maps can be helpful in this regard but only if the individual map units and borders conform to actual soil drainage contours. To this extent, further progress can be made by:

1) refining and adjusting each unit to its landform- and DEM-defining drainage position;

2) exploring how the trafficability affecting soil properties (*MC*, texture, *CF*, *OM*, *Db*, depth) vary across the landscape of interest from the highest to the lowest elevation points;

3) determining the point of streamflow initiation inside each flow channel either through field observations or through DEM-based flow-initiation algorithms.

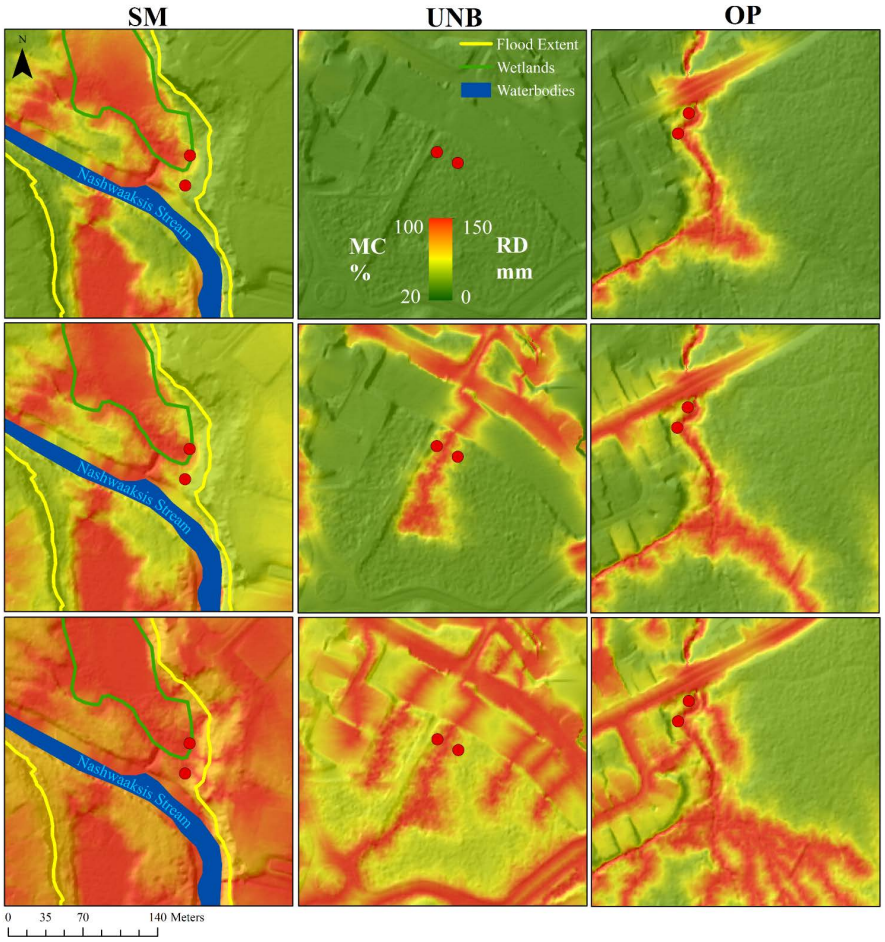

Figure 11. Soil moisture content per pore space [MC_{ps} (%)] and all-terrain rut depth after 10 passes along same track (RD_{10}, mm), generated from the season–representative *DTW* patterns in **Figure 10** using Equation (7) and Equation (8). Top: end-of summer. Middle: spring-to-summer and fall-to-winter transitions. Bottom: after snowmelt.

Together, these refinements would add further precision to the soil moisture and rut depth maps in **Figure 11**. For example, there would be a noticeable difference between *DTW*, MC_{ps} and *ATV* rut depth projections within and outside the floodplain associated with the *SM* location.

Some progress towards these refinements has already been made in terms of checking existing trail conditions in terms of *ATV*-induced rutting extent, and by correlating this extent to the ridge-to-valley of the cartographic depth-to-water index (*DTW* [40]). The multi-pass implications on wood-forwarding rutting depth have been reported by [56], and were further evaluated by [4] by way of Equation (7) and Equation (8). However, much more work needs to be done by not only addressing the *DTW*-emulated variations in soil wetness but also by addressing the changes in D_b, texture, *CF* and *OM* content as these would vary from ridge tops to valleys in a systematic manner. For example, upslope soils would generally be thinner and coarser with less *OM* than downslope soils. The reverse would occur in severely eroded medium-textured soils, with the more cohesive soil remains upslope and the more easily eroding sand and silt fractions

accumulating downslope.

Since the above analysis is restricted to bare ground conditions and mineral soil layers, rut-reducing surface accumulations of snow, ice, forest litter, peat, and roots are not addressed. Bare-ground conditions, however, exist across forested landscapes along non-paved roads, after ground-exposing operations such as root extractions, mounding and plowing, and underneath forest cover where litter accumulations are low or absent due to fast litter decomposition rates. The latter condition is more prevalent under hardwood and pine forests than under fir and spruce forests. Repeated recreational traffic in such areas under moist to wet weather conditions would induce significant rut-induced damage through trail braiding, soil erosion, gulley formation, and stream and lake sedimentation [45].

Also not addressed are the effects of snow and ice build-up on top of soils during winter, which would increase the resistance to soil penetration, compaction, and rutting through increased load-bearing capacities. Since not all the water is frozen in sub-zero clay- and *OM*-enriched soils, there could be problems associated winter-based soil rutting followed by instantaneous flash freezing. In summary, the above soil rutting assessment is only applicable for bare ground conditions. Soils covered by forest litter, slash, snow, and ice would obviously reduce rutting.

5. Concluding Remarks

The above soil rutting assessment via manual testing of the temporal changes in the soil resistance to penetration is limited to the immediate area at and around the three sampling locations of this study. More research is needed to extend and test this research regarding general applicability. As shown, the approach taken would allow this by way of hydrological and digital elevation modelling, and further procurement of *CI*-relevant soil information.

Acknowledgements

This research was supported by a Collaborative Research Developement Project sponsored by J.D. Irving, Limited, and the Natural Science and Engineering Council of Canada. Special thanks go to Doug Hiltz, Friedrich Wüthrich, and Brittany Hartery for weekly field sampling.

References

[1] Eid, H.T. and Stark, T.D. (1998) Undrained Shear Strength for Cone Penetration Tests. In: Robertson and Mayne, Eds., *Geotechnical Site Characterization*, Balkema, Rotterdam.

[2] Lowery, B. and Morrison, J.E. (2002) Soil Penetrometers and Penetrability. In: *Methods of Soil Analysis*, *Part* 4. *Physical Methods*, Soil Science Society of America, Inc., Madison, WI, 363-385.

[3] Balland, V., Pollacco, J.A.P. and Arp, P.A. (2008) Modeling Soil Hydraulic Properties for a Wide Range of Soil Conditions. *Ecological Modelling*, **219**, 300-316.

[4] Vega-Nieva, D.J.D., Murphy, P.N.C., Castonguay, M., Ogilvie, J. and Arp, P.A. (2009) A Modular Terrain Model for Daily Variations in Machine-Specific Forest Soil Trafficability. *Canadian Journal of Soil Science*, **89**, 93-109. https://doi.org/10.4141/CJSS06033

[5] Vaz, C.M.P., Manieri, J.M., de Maria, I.C. and Tuller, M. (2011) Modeling and Correction of Soil Penetration Resistance for Varying Soil Water Content. *Geoderma*, **166**, 92-101.

[6] Lin, J., Sun, Y. and Schulze Lammers, P. (2014) Evaluating Model-Based Relationship of Cone Index, Soil Water Content and Bulk Density Using Dual-Sensor Penetrometer Data. *Soil and Tillage Research*, **138**, 9-16.

[7] Brady, N.C. and Weil, R.R. (2008) The Nature and Properties of Soils. 14th Edition, Prentice Hall, Upper Saddle River, NJ.

[8] Kumar, A., Chen, Y., Sadek, A. and Rahman, S. (2012) Soil Cone Index in Relation to Soil Texture, Moisture Content, and Bulk Density for No-Tillage and Conventional Tillage. *Agriculture Engineering International*: *CIGR Journal*, **14**, 26-37.

[9] Andersland, O.B. and Ladanyi, B. (1994) Mechanical Properties of Frozen Soils. In: *An Introduction to Frozen Ground Engineering*, Springer, US, 121-150. https://doi.org/10.1007/978-1-4757-2290-1_5

[10] Bronick, C.J. and Lal, R. (2005) Soil Structure and Management: A Review. *Geoderma*, **124**, 3-22.

[11] Huntington, T.G. (2007) Available Water Capacity and Soil Organic Matter. In: *Encyclopedia of Soil Science*, 139-143.

[12] Culley, J.L., Dow, B.K., Presant, E.W. and Maclean, A. (1981) Impacts of Installation of an Oil Pipeline on the Productivity of Ontario Cropland. Research Branch, Agriculture Canada.

[13] Soane, B.D. and van Ouwerkerk, C. (1994) Soil Compaction Problems in World Agriculture. In: *Soil Compaction in Crop Production*, 1-9.

[14] Chen, G. and Weil, R.R. (2010) Penetration of Cover Crop Roots through Compacted Soils. *Plant and Soil*, **331**, 31-43. https://doi.org/10.1007/s11104-009-0223-7

[15] Chen, G. and Weil, R.R. (2011) Root Growth and Yield of Maize as Affected by Soil Compaction and Cover Crops. *Soil and Tillage Research*, **117**, 17-27.

[16] Gregory, J., Dukes, M., Jones, P. and Miller, G. (2006) Effect of Urban Soil Compaction on Infiltration Rate. *Journal of Soil and Water Conservation*, **61**, 117-124.

[17] Kozlowski, T.T. (2008) Soil Compaction and Growth of Woody Plants. *Scandinavia Journal of Forest Resources*, **14**, 596-619. https://doi.org/10.1080/02827589908540825

[18] Moehring, D.M. and Rawls, I.W. (1970) Detrimental Effects of Wet Weather Logging. *Journal of Forestry*, **68**, 166-167.

[19] Carter, E.A., Aust, W.M. and Burger, J.A. (2007) Soil Strength Response of Select Soil Disturbance Classes on a Wet Pine Flat in South Carolina. *Forest Ecology and Management*, **247**, 131-139.

[20] Saarilahti, M. (2002) Soil Interaction Model—Development of a Protocol for Ecoefficient Wood Harvesting on Sensitive Sites (Ecowood). Appendix Report No. 5.

[21] Affleck, R.T. (2005) Disturbance Measurements from Off-Road Vehicles on Seasonal Terrain Cold Regions Research and Engineering Laboratory. US Army Corps of Engineers, Engineer Research and Development Center, Cold Regions Research and Engineering Laboratory.

[22] Sakai, H., Nordfjell, T., Suadicani, K., Talbot, B. and Bøllehuus, E. (2008) Soil

Compaction on Forest Soils from Different Kinds of Tires and Tracks and Possibility of Accurate Estimate. *Croatian Journal of Forest Engineering*, **29**, 15-27.

[23] Han, H.-S., Page-Dumroese, D., Han, S.-K. and Tirocke, J. (2006) Effects of Slash, Machine Passes, and Soil Moisture on Penetration Resistance in a Cut-to-Length Harvesting. *International Journal of Forest Engineering*, **17**, 11-24.

[24] Shoop, S.A. (1995) Vehicle Bearing Capacity of Frozen Ground over a Soft Substrate. *Canadian Geotechnical Journal*, **32**, 552-556. https://doi.org/10.1139/t95-057

[25] Robertson, P.K. (2016) Cone Penetration Test (CPT)-Based Soil Behaviour Type (SBT) Classification System—An Update. *Canadian Geotechnical Journal*, **53**, 1910-1927. https://doi.org/10.1139/cgj-2016-0044

[26] Stobbe, P.C. (1940) Soil Survey of Fredericton-Gagetown Area. Department of Agriculture, Experimental Farm Service, 51 p.

[27] Department of Environment and Climate Change Canada (2016) Historical Climate Data. http://climate.weather.gc.ca/

[28] Shelrick, B.H. and Wang, C. (1993) Particle Size Distribution. In: Carter, M.C., Ed., *Soil Sampling and Methods of Analysis*, Lewis Publishers, Boca Raton, FL.

[29] Arp, P.A. and Yin, X. (1992) Predicting Water Fluxes through Forest from Monthly Precipitation and Mean Monthly Air Temperature Records. *Canadian Journal of Forest Research*, **22**, 864-877. https://doi.org/10.1139/x92-116

[30] Yin, X. and Arp, P.A. (1994) Fog Contributions to the Water Budget of Forested Watersheds in the Canadian Maritime Provinces: A Generalized Algorithm for Low Elevations. *Atmosphere-Ocean*, **32**, 553-565. https://doi.org/10.1080/07055900.1994.9649512

[31] Jutras, M.-F. (2012) Modeling Stream Discharge in Forest Catchments across Canada: Hydraulic Conductivity Calibrations. Unpublished Master's Thesis, University of New Brunswick, Canada.

[32] Department of Environment and Climate Change Canada (2016) Historical Hydrometric Data. http://wateroffice.ec.gc.ca/

[33] Balland, V., Bhatti, J., Errington, R., Castonguay, M. and Arp, P.A. (2006) Modeling Snowpack and Soil Temperature and Moisture Conditions in a Jack Pine, Black Spruce and Aspen Forest Stand in Central Saskatchewan (BOREAS SSA). *Canadian Journal of Soil Science*, **86**, 203-217. https://doi.org/10.4141/S05-088

[34] Jutras, M.-F. and Arp, P.A. (2010) Determining Hydraulic Conductivity from Soil Characteristics with Applications for Modelling Stream Discharge in Forest Catchments. In: Elango, L., Ed., *Hydraulic Conductivity—Issues, Determination and Applications*, InTech, 189-202.

[35] Jutras, M.-F. and Arp, P.A. (2013) Role of Hydraulic Conductivity Uncertainties in Modeling Water Flow through Forest Watersheds. In: Rodrigues da Silva, V., Ed., *Hydraulic Conductivity*, InTech, 33-54. https://doi.org/10.5772/56900

[36] Saarilahti, M. (2002) Soil Interaction Model—Development of a Protocol for Ecoefficient Wood Harvesting on Sensitive Sites (Ecowood). Appendix No. 8 Forest Soil Properties.

[37] GeoNB (2015) Bare-Earth Digital Elevation Model. Service New Brunswick, Fredericton, NB.

[38] Murphy, P.N.C., Ogilvie, J. and Arp, P.A. (2009) Topographic Modelling of Soil Moisture Conditions: A Comparison and Verification of Two Models. *European Journal of Soil Science*, **60**, 94-109. https://doi.org/10.1111/j.1365-2389.2008.01094.x

[39] White, B., Ogilvie, J., Campbell, D.M.H., Hiltz, D., Gauthier, B., Chisholm, H.K.H.,

Wen, H.K., Murphy, P.N.C. and Arp, P.A. (2012) Using the Cartographic Depth-to-Water Index to Locate Small Streams and Associated Wet Areas across Landscapes. *Canadian Water Resources Journal*, **37**, 333-347. https://doi.org/10.4296/cwrj2011-909

[40] Murphy, P.N.C., Castonguay, M., Ogilvie, J., Nasr, M., Hazlett, P., Bhatti, J.S. and Arp, P.A. (2009) A Geospatial and Temporal Framework for Modeling Gaseous N and Other N Losses from Forest Soils and Basins, with Application to the Turkey Lakes Watershed Project, in Ontario, Canada. *Forest Ecology and Management*, **258**, 2304-2317.

[41] Young, G.C. and Berlyn, R.W. (1968) Some Variations in Soil Trafficability as Measured with a Cone Penetrometer. Pulp and Paper Research Institute of Canada, Pointe Claire, P.Q.

[42] Busscher, W.J., Bauer, P.J., Camp, C.R. and Sojka, R.E. (1997) Correction of Cone Index for Soil Water Content Differences in a Coastal Plain Soil. *Soil and Tillage Research*, **43**, 205-217.

[43] Carter, E., McDonald, T. and Torbert, J. (2000) Assessment of Soil Strength Variability in a Harvested Loblolly Pine Plantation in the Piedmon Region of Alabama, United States. *New Zealand Journal of Forestry Science*, **30**, 237-279.

[44] Porsinsky, T., Sraka, M. and Stankic, I. (2006) Comparison of Two Approaches to Soil Strength Classifications. *Croatian Journal of Forest Engineering*, **27**, 17-26.

[45] Campbell, D.M.H., White, B. and Arp, P.A. (2013) Modeling and Mapping Soil Resistance to Penetration and Rutting Using LiDAR-Derived Digital Elevation Data. *Journal of Soil and Water Conservation*, **68**, 460-473. https://doi.org/10.2489/jswc.68.6.460

[46] Baetens, J.M., Verbist, K., Cornells, W.M., Gabriels, D. and Soto, G. (2009) On the Influence of Coarse Fragments on Soil Water Retention. *Water Resources Research*, **45**, W07408. https://doi.org/10.1029/2008WR007402

[47] Rücknagel, J., Götze, P., Hofmann, B., Christen, O. and Marschall, K. (2013) The Influence of Soil Gravel Content on Compaction Behaviour and Pre-Compression Stress. *Geoderma*, **209-210**, 226-232.

[48] Alexander, L. and Skaggs, R.W. (1987) Predicting Unsaturated Hydraulic Conductivity from Soil Texture. *Journal of Irrigation and Drainage Engineering*, **113**, 184-197. https://doi.org/10.1061/(ASCE)0733-9437(1987)113:2(184)

[49] Wesseling, J.G., Stoof, C.R., Ritsema, C.J., Oostindie, K. and Dekker, L.W. (2009) The Effect of Soil Texture and Organic Amendment on the Hydrological Behaviour of Coarse-Textured Soils. *Soil Use and Management*, **25**, 274-283. https://doi.org/10.1111/j.1475-2743.2009.00224.x

[50] Manuwa, S.I. (2012) Evaluation of Shear Strength and Cone Penetration Resistance Behavior of Tropical Silt Loam Soil under Uni-Axial Compression. *Open Journal of Soil Science*, **2**, 95-99. https://doi.org/10.4236/ojss.2012.22014

[51] Hausenbuilder, R.L. (1978) Soil Science: Principles and Practices. 2nd Edition, William C. Brown Company, Reading, PA.

[52] Krzic, M., Bulmer, C.E., Teste, F., Dampier, L. and Rahman, S. (2004) Soil Properties Influencing Compactability of Forest Soils in British Columbia. *Canadian Journal of Soil Science*, **84**, 219-226. https://doi.org/10.4141/S03-056

[53] Šušnjar, M., Horvat, D. and Šešelj, J. (2006) Soil Compaction in Timber Skidding in Winter Conditions. *Croatian Journal of Forest Engineering*, **1**, 3-15.

[54] Jakobsen, B.F. and Dexter, A.R. (1987) Effect of Soil Structure on Wheat Root Growth, Water Uptake and Grain Yield. A Computer Simulation Model. *Soil and*

Tillage Research, **10**, 331-345.

[55] Busscher, W.J., Spivey, L.D. and Campbell, R.B. (1987) Estimation of Soil Strength Properties for Critical Rooting Conditions. *Soil and Tillage Research,* **9**, 377-386.

[56] Meek, P. (1996) Effects of Skidder Traffic on Two Types of Forest Soils. Technical Report No. TR_117, Pointe-Claire, QC.

Open Journal of Soil Science

ISSN: 2162-5360 (Print) ISSN: 2162-5379 (Online)
http://www.scirp.org/journal/ojss

***Open Journal of Soil Science* (OJSS)** is an international journal dedicated to the latest advancement of soil science. The goal of this journal is to provide a platform for scientists and academicians all over the world to promote, share, and discuss various new issues and developments in different areas of soil science.

Editor-in-Chief

Editorial Board

Subject Coverage

This journal invites original research and review papers that address the following issues in soil science. Topics of interest include, but are not limited to:

- Soil and Global Change
- Soil Biology and Biochemistry
- Soil Chemistry
- Soil Ecology
- Soil Environment
- Soil Fertility and Plant Nutrition
- Soil Geography
- Soil Improvement Studies
- Soil Microbiology
- Soil Physics
- Soil Remediation
- Soil Resources and Use
- Soil Science in Other Disciplines
- Soil Survey and Evaluation
- Soil Taxonomy
- Soil Tillage

We are also interested in short papers (letters) that clearly address a specific problem, and short survey or position papers that sketch the results or problems on a specific topic. Authors of selected short papers would be invited to write a regular paper on the same topic for future issues of the ***OJSS***.

Notes for Intending Authors

Submitted papers should not have been previously published nor be currently under consideration for publication elsewhere. Paper submission will be handled electronically through the website. All papers are refereed through a peer review process. For more details about the submissions, please access the website.

Website and E-Mail

http://www.scirp.org/journal/ojss Email: ojss@scirp.org

What is SCIRP?

Scientific Research Publishing (SCIRP) is one of the largest Open Access journal publishers. It is currently publishing more than 200 open access, online, peer-reviewed journals covering a wide range of academic disciplines. SCIRP serves the worldwide academic communities and contributes to the progress and application of science with its publication.

What is Open Access?

All original research papers published by SCIRP are made freely and permanently accessible online immediately upon publication. To be able to provide open access journals, SCIRP defrays operation costs from authors and subscription charges only for its printed version. Open access publishing allows an immediate, worldwide, barrier-free, open access to the full text of research papers, which is in the best interests of the scientific community.

- High visibility for maximum global exposure with open access publishing model
- Rigorous peer review of research papers
- Prompt faster publication with less cost
- Guaranteed targeted, multidisciplinary audience

Scientific Research Publishing

Website: http://www.scirp.org

Subscription: sub@scirp.org

Advertisement: service@scirp.org